Review of Materials Research 1 (2025) 100017

Contents lists available at ScienceDirect

Review of Materials Research

journal homepage: www.sciencedirect.com/journal/review-of-materials-research

Self-assembled monolayers for perovskite solar cells

Weifei Fu [a,b], Ahmed I.A. Soliman [a,c], Yiran Zheng [a], Yu Zhou [a], Yiqing Zhang [a], Shiqi Shan [a], Hongzheng Chen [a,b,*]

[a] State Key Laboratory of Silicon and Advanced Semiconductor Materials, Department of Polymer Science and Engineering, Zhejiang University, Hangzhou, 310058, China
[b] Zhejiang University-Hangzhou Global Scientific and Technological Innovation Center, Hangzhou, 311200, China
[c] Chemistry Department, Faculty of Science, Assiut University, Assiut, 71516, Egypt

ARTICLE INFO

Keywords:
Self-assembled monolayers
Perovskite solar cells
Interfaces
Stability

ABSTRACT

Self-assembled monolayers (SAMs) have emerged as an effective and promising interface engineering approach to enhance the performance and stability in perovskite solar cells (PVSCs). In recent years, they have gained significant attention due to their advantages of minimal light absorption, low material consumption, simple processing, and conformal coating. By optimizing the energy level alignment, suppressing interface defects, boosting charge extraction, and improving resistance to moisture and oxygen, highly efficient and stable PVSCs have been successfully achieved. In this review, we provide a comprehensive summary of the development and progress of SAMs for interfacial engineering in PVSCs. We specifically discuss strategies for growing high-quality SAM films on various interfaces with desired properties, highlighting the key principles for selecting, designing, and optimizing SAMs for different interfaces in the context of device fabrication. Finally, we offer perspectives on the future development of SAMs to further enhance PVSC performance and stability, thereby advancing their commercialization.

1. Introduction

Due to the advantages of high performance, low cost, and simple manufacturing process, perovskite solar cells (PVSCs) are among the most promising new-generation solar technologies [1]. In the past years, the power conversion efficiencies (PCEs) of PVSCs have increased rapidly up to 27.0% [2]. Further increasing the performance and enhancing the stability of the devices are significantly important for their commercialization [3]. Optimizing the properties of interfaces such as electrode/perovskite and charge transporting layer (CTL)/perovskite in PVSCs is one of the efficient strategies to achieve this goal [4,5].

Poly(3,4-ethylenedioxythiophene): polystyrene sulfonate (PEDOT:PSS) [6], poly[bis(4-phenyl)(2,4,6-trimethylphenyl)amine (PTAA) [7], metal oxides such as molybdenum oxide (MoO_3) [8], nickel oxide (NiO_x) [9,10] are widely used as hole-transporting layers (HTLs), while TiO_x [11], ZnO [12], SnO_2 [13] and conjugated polyelectrolytes [14] are widely used as electron-transporting layers (ETLs) in PVSCs. On the other hand, self-assembled monolayers (SAMs) are another kind of promising alternatives for traditional charge transporting materials due to the electronic properties tuning ability of the interfaces, minimal absorption, low material consumption and simple processing [15]. Furthermore, these SAMs are beneficial to the morphology control, defects passivation for electrodes, CTLs and perovskite layers to further improve the device performance and stability, and thus are widely used in PVSCs [16]. They have also been investigated extensively as efficient interface layers for highly efficient electronics such as organic solar cells (OSCs) [15,17,18], organic light-emitting diodes [19] and organic field-effect transistors [19,20]. For example, Guan et al. [18] recently achieved OSCs with a PCE of 20.17% (19.79% certified) using 2-(9H-carbazol-9-yl) (2PACz) SAM-modified indium tin oxide (ITO).

In this review, we provide a comprehensive summary of the development and progress of SAMs for interfacial engineering in PVSCs. We focus on strategies for growing high-quality SAMs on different interfaces, emphasizing the key principles for selecting, designing, and optimizing SAMs with desired properties, in the context of device fabrication. We also provide insights into the future development of SAMs to further enhance PVSC performance and stability, paving the way for their commercialization.

* Corresponding author. State Key Laboratory of Silicon and Advanced Semiconductor Materials, Department of Polymer Science and Engineering, Zhejiang University, Hangzhou, 310058, China.
E-mail address: hzchen@zju.edu.cn (H. Chen).

https://doi.org/10.1016/j.revmat.2025.100017
Received 22 March 2025; Received in revised form 7 April 2025; Accepted 7 April 2025
Available online 8 April 2025

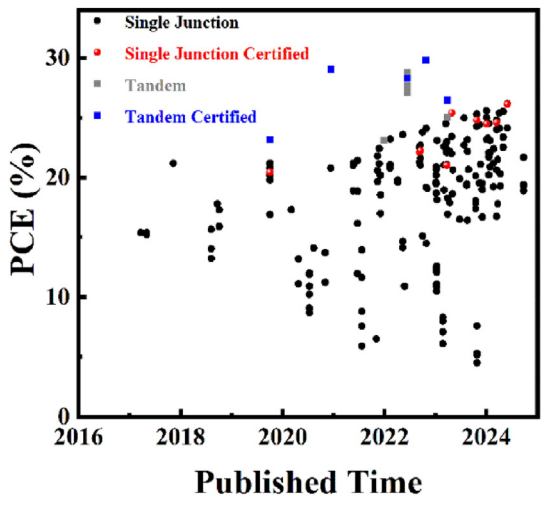

Fig. 1. The evolution of PCEs of PVSCs based on SAMs modified ITO.

2. Modification of ITO by SAMs in PVSCs

Due to the work function (WF) tuning ability, SAMs could provide Ohmic contact at ITO (or fluorine-doped tin oxide (FTO))/perovskite interfaces to ensure the efficient charge extraction for high short-circuit current density (J_{SC}) and fill factor (FF). It is also necessary to match the WF of the modified ITO with the valence band maximum (VBM) of perovskite to realize maximum open-circuit voltage (V_{OC}). In recent research of PVSCs, SAMs have been widely used to modify ITO for hole/electron extraction, achieving rapid progress (Fig. 1). The chemical structures of the reported molecules used to modify ITO in n-i-p and p-i-n PVSCs are shown in Figs. 2 and 3, respectively. The device structures, photovoltaic parameters and stabilities are listed in Table 1 and Table S1.

2.1. The development of SAMs for ITO modification in PVSCs

Hou et al. [21] modified ITO with C_{60}-based phosphonic acid (C_{60}-C6-PA) and 3-iodophenylphosphonic acid (I-Ph-PA) co-assembled monolayer (co-SAM) for n-i-p PVSCs in 2017. In their work, the mixed phosphonic acids yielded a complete and well-organized surface coverage on ITO, with a sufficient fullerene density for improved electronic properties due to the balanced chain length of C_{60}-C6-PA and the support I-Ph-PA. Thus, the PVSCs based on the co-SAM show higher PCE with reduced hysteresis compared to the device based on TiO_2. There are only a few works on SAMs as electron extraction layers in PVSCs [22–26].

The most successfully and widely used SAMs for p-i-n PVSCs are based on carbazole-based phosphonic acids. Magomedov et al. [27] synthesized (2-(3,6-bis[bis(4-methoxyphenyl)amino]-9H-carbazol-9-yl) ethyl)phosphonic acid (V1036) with a phosphonic acid anchoring group and dimethoxydiphenylamine substituted carbazole fragment to modify ITO in p-i-n PVSCs in 2018. By changing the molar ratio of V1036 and butylphosphonic acid (C4), the surface properties such as WF, wettability of the modified ITO could be tuned. The optimized device shows a PCE of 17.8%, which is lower than that of the device with PTAA (19.2%) as HTL [27]. Later, they developed [2-(3,6-dimethoxy-9H-carbazol-9-yl)ethyl] phosphonic acid (MeO-2PACz) and 2PACz, who are energetically more hole-selective than PTAA due to the higher energetic barrier for electrons, while still allowing for an efficient extraction of holes (no barrier) (Fig. 4a). Thus 2PACz based PVSC shows a highest PCE of 20.9% [28]. Later, they compared methoxy and methyl substituents in p-i-n PVSCs with MeO-2PACz and ([4-(3,6-dimethyl-9H-carbazol-9-yl)butyl]phosphonic acid) (Me-4PACz), which show advantages of the methyl substitution with respect to both passivation and hole extraction [29]. This was also demonstrated by Levine et al. by utilizing steady-state and transient surface photovoltage (Fig. 4b) [30]. The fast charge extraction and good passivation ability of Me-4PACz improve the device performance and enhance the phase stability of 1.68 eV wide-bandgap (WBG) perovskite with 23% Br [29].

After years of development, the PCEs higher than 25% have been achieved for p-i-n PVSCs, with excellent operational stability [32–34,42, 51]. In the following sections, strategies for growing high-quality SAM films on ITO with desired properties will be discussed.

2.2. Wettability

Although the Me-4PACz based devices showed excellent performance, the wide use of Me-4PACz is hindered by the rather poor coverage of perovskite films due to the wettability issue. Several strategies have been developed to overcome this disadvantage. Kulkarni et al. [83] found that the incorporation of N-methyl-2-pyrrolidone (NMP) into dimethylformamide (DMF) and dimethyl sulfoxide (DMSO) could improve the interaction between the perovskite ink and Me-4PACz coated substrate and thus a uniform perovskite layer could be obtained. Tockhorn et al. [84] found that when the perovskite is spin-coated onto nanotextured silicon bottom cells covered with Me-4PACz, the occurrence of macroscopic holes is strongly reduced, improving the sample yield from ~50% to ~95%. Taddei et al. [85] and Perera et al. [86] employed Al_2O_3 nanoparticles on top of Me-4PACz layer to improve the perovskite solution wetting. Ashouri et al. [54] found that adding a second component, 1,6-hexylenediphosphonic acid (6dPA), to the Me-4PACz precursor could substantially improve the wetting, leading to only 8% of the pixels being shunted from 67% (Fig. 4c). Farag et al. [87] found that evaporated Me-4PACz surface exhibits significantly lower contact angle compared to the solution-processed counterpart. This enhanced surface wettability leads to improved surface coverage for solution-processed perovskite films and thus ~100% fabrication yield. Hossain et al. [88] reported a mixing engineering strategy which adds poly(9,9-bis(3'-(N,

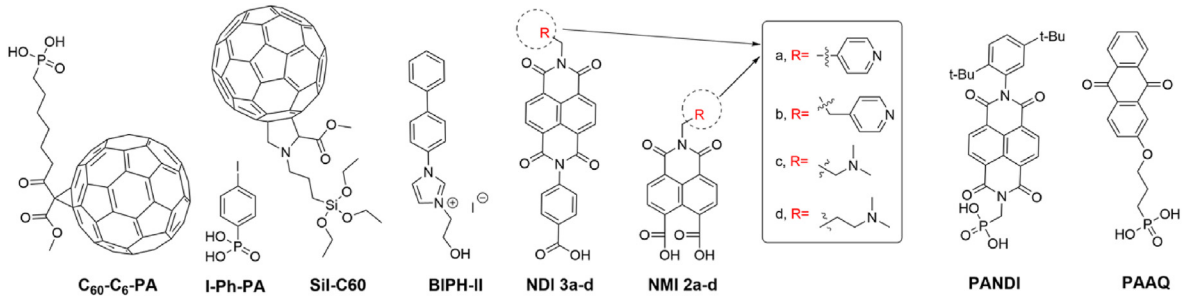

Fig. 2. Chemical structures of SAM molecules used to modify ITO in n-i-p PVSCs: C_{60}-C_6-PA and I-Ph-PA [21,22], *N*-[3-(triethoxysilyl)propyl]-2-carbomethoxy-3, 4-fulleropyrrolidine (Sil-C60) [23], hydroxyethyl-functionalized imidazolium iodide (BIPH-II) [24], naphthalene-1,8:4,5-bis(dicarboximide)s (NDI 3a-d) and naphthalene-1,8-dicarbox-imide-4,5-dicarboxylic acids (NMI 2a-d) [25], *N*-(2,5-di-*tert*-butylphenyl)-*N'*-(methyl)-1,4,5,8-naphthalene tetracarboxylic di-imide phosphonic acid (PANDI) and 3-[(9,10-dioxo-9,10-dihydroan-thracen-2-yl)oxy]propyl phosphonic acid (PAAQ) [26].

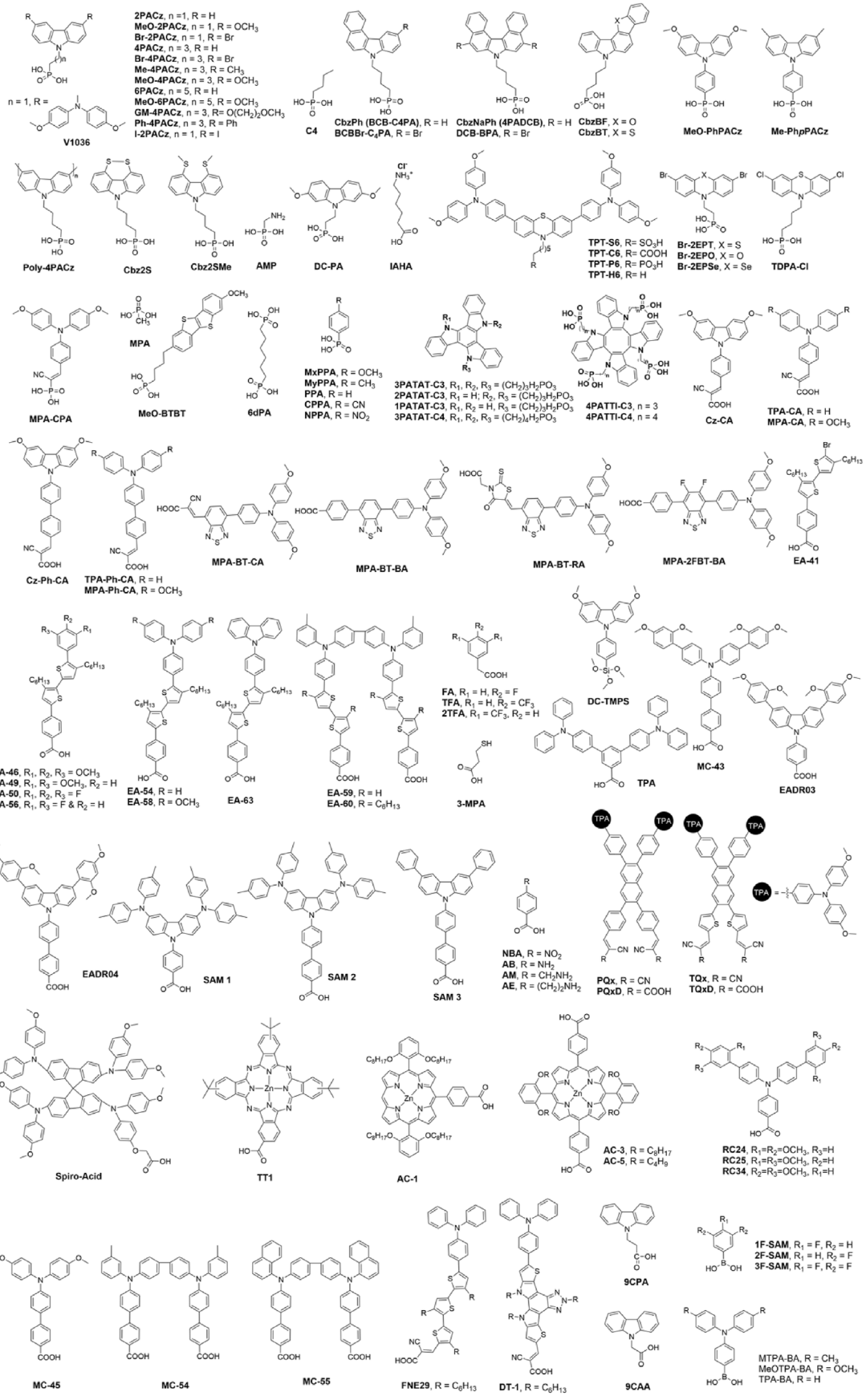

(caption on next page)

Fig. 3. Chemical structures of SAM molecules used to modify ITO in p-i-n PVSCs: V1036 and C4 [27], MeO-2PACz and 2PACz [28], Me-4PACz, 6PACz, and Me-6PACz [29], 4PACz [30], Br-2PACz [31], MeO-4PACz, GM-4PACz [32], Ph-4PACz [33], I-2PACz [34], CbzPh (BCB-C4PA) and CbzNaph (4PADCB) [35–37], BCBBr-C4PA [38], (4-(5,9-dibromo-7*H*-dibenzo[*c*,*g*]carbazol-7-yl)butyl)phosphonic acid (DCB-BPA) [39], CbzBF and CbzBT [40], MeO-PhPACz [41], Me-Ph*p*PACz [42], Poly-4PACz [43], Cbz2S and Cbz2SMe [44], AMP [45], DC-PA and IAHA [46], TPT-H6, TPT-S6, TPT-C6, and TPT-P6 [47], Br-2EPT [48], Br-2EPO and Br-2EPSe [49], TDPA-Cl [50], MPA-CPA [51], MPA [52], MeO-BTBT [53], 6dPA [54], 4-methoxyphenylphosphonic acid (MxPPA), 4-methylphenylphosphonic acid (MyPPA), phenylphosphonic acid (PPA), 4-cyanophenylphosphonic acid (CPPA), and 4-nitrophenylphosphonic acid (NPPA) [55], 3PATAT-C3, 2PATAT-C3, 1PATAT-C3 and 3PATAT-C4 [56], 4PATTI-C3 and 4PATTI-C4 [57], Cz-CA, Cz-Ph-CA, TPA-CA, TPA-Ph-CA, MPA-CA and MPA-Ph-CA [58], MPA-BT-CA, MPA-BT-BA and MPA-BT-RA [59], MPA-2FBT-BA [60], EA-41, EA-46, EA-49, EA-50 and EA-56 [61], EA-54, EA-58 and EA-63 [62], EA-59 and EA-60 [63], 4-fluorophenylacetic acid (FA), 4-(trifluoromethyl)phenylacetic acid (TFA), and 3,5-bis(trifluoromethyl)phenylacetic acid (2TFA) [64], 3-MPA [65], DC-TMPS [66], TPA and 4'-[bis(2′,4′-dimethoxybiphenyl-4-yl)amino]-biphenyl-4-carboxylic acid (MC-43) [67], 4-(3,6-bis(2,4-dimethoxyphenyl)-9*H*-carbazol-9-yl)benzoic acid (EADR03) and 4'-(3,6-bis(2,4-dimethoxyphenyl)-9*H*-carbazol-9-yl)-[1,1′-biphenyl]-4-carboxylic acid (EADR04) [68], SAM1, SAM2 and SAM3 [69], 4-nitrobenzoic acid (NBA) [70], 4-aminobenzoic acid (AB), 4-(2-aminomethyl)benzoic acid (AM) and 4-(2-aminoethyl)benzoic acid (AE) [71], PQx, TQx, PQxD and TQxD [72], spiro-acid [73], TT1 [74], AC-1, AC-3 and AC-5 [75], RC24, RC25 and RC34 [76], MC-45, MC-54 and MC-55 [77], FEN29 and DT-1 [78], 9CPA and 9CAA [79], 1F-SAM, 2F-SAM and 3F-SAM [80], MTPA-BA, MeOTPA-BA and TPA-BA [81].

N-dimethyl)-N-ethylammonium-propyl-2,7-fluorene)-alt-2,7-(9,9-dioctylfluorene)) dibromide (PFN-Br), to the Me-4PACz to obtain a uniform perovskite film. Liu et al. [89] found that incorporation of PFN-Br between MeO-2PACz and perovskite could also improve the reproducibility of PVSCs. Zheng et al. [90] and Wang et al. [36] demonstrated that incorporating SAM molecules into perovskite precursors could solve the critical wetting issues when processing perovskite on SAMs, and this strategy could also simplify the manufacturability. Zhou et al. [32] synthesized [4-(3,6-glycol monomethyl ether-9*H*-carbazol-9-yl)butyl]phosphonic acid (GM-4PACz) by introducing glycol monomethyl ether side chains at carbazolyl unit to improve the wetting ability of SAM modified ITO. Furthermore, the glycol monomethyl ether chain in GM-4PACz successfully passivate the buried surface defects of perovskite by Lewis acid-base interaction and hydrogen bond, and further release the residual interface stress. In addition to Me-4PACz, other carbazole-based SAMs also suffer from the wettability issue. Cassella et al. [91] used the optimized solvent rinsing protocol to overcome the dewetting issue of MeO-2PACz. Vidyasagar et al. [92] found that treatment of 2PACz using high donor number solvents, such as DMSO, could leave surface-bound DMSO molecules on 2PACz to enhance the wettability. Song et al. [93] found that a tin-based perovskite layer could be deposited by a two-step procedure on the hydrophobic MeO-2PACz SAM. Pitaro et al. [31] introduced a layer of a carbazole alkylammonium iodide derivative ($4CzNH_3I$) on top of (2-(3,6-Dibromo-9H-carbazol-9-yl)ethyl)phosphonic acid (Br-2PACz) to increase the hydrophilicity of the surface and also passivate the buried interface of perovskite films, thus improving the fabrication yield and enabling the large-area devices.

In most cases, the SAMs modification will increase the hydrophobicity of ITO, and thus larger grains and enhanced crystallinity of perovskite were observed in some reported works [21,23,46], while

Table 1
A selected summary of the device structures, photovoltaic parameters and stabilities of PVSCs based on SAMs modified ITO.

Device Structure	PCE [%]	Stability	Ref
ITO/PTAA/$Cs_{0.05}(MA_{0.17}FA_{0.83})_{0.95}Pb(I_{0.83}Br_{0.17})_3$/PCBM/Ag	19.2	w/o encapsulation, N_2, dark, keep ~95% after 180 days	[27]
ITO/V1036:C4/$Cs_{0.05}(MA_{0.17}FA_{0.83})_{0.95}Pb(I_{0.83}Br_{0.17})_3$/PCBM/Ag	17.8	w/o encapsulation, N_2, dark, keep ~94% after 180 days	
ITO/V1036/$Cs_{0.05}(MA_{0.17}FA_{0.83})_{0.95}Pb(I_{0.83}Br_{0.17})_3$/$C_{60}$/BCP/Cu	16.9	N_2, MPP tracking, 40 °C, keep ~88% after 11 h	[28]
ITO/MeO-2PACz/$Cs_{0.05}(MA_{0.17}FA_{0.83})_{0.95}Pb(I_{0.83}Br_{0.17})_3$/$C_{60}$/BCP/Cu	20.2	N_2, MPP tracking, 40 °C, keep ~97% after 11 h	
ITO/2PACz/$Cs_{0.05}(MA_{0.17}FA_{0.83})_{0.95}Pb(I_{0.83}Br_{0.17})_3$/$C_{60}$/BCP/Cu	20.8 (20.44% certified)	N_2, MPP tracking, 40 °C, keep >97% after 11 h	
Si solar cell/ITO/PTAA/$Cs_{0.05}(MA_{0.23}FA_{0.77})_{0.95}Pb(I_{0.77}Br_{0.23})_3$/LiF/$C_{60}$/$SnO_2$/IZO/Ag/LiF	26.79	w/o encapsulation, MPP tracking, 25 °C, 30–40% humidity, keep 74.5% after 90 h	[29]
Si solar cell/ITO/Me-4PACz/$Cs_{0.05}(MA_{0.23}FA_{0.77})_{0.95}Pb(I_{0.77}Br_{0.23})_3$/LiF/$C_{60}$/$SnO_2$/IZO/Ag/LiF	29.05 (certified, 1.064 cm^2)	w/o encapsulation, MPP tracking, 25 °C, 30–40% humidity, keep 75.9% after 300 h	
ITO/GM-4PACz/$Cs_{0.05}(FA_{0.95}MA_{0.05})_{0.95}Pb(I_{0.95}Br_{0.05})_3$/$PC_{61}BM$/BCP/Ag	25.52	w/o encapsulation, 25 °C, 30% humidity, keep 93.29% after 2000 h; 85 °C, N_2, keep 88.13% after 500 h; encapsulated, MPP tracking, keep 91.75% after 1000 h	[32]
FTO/Me-4PACz/$Cs_{0.05}(FA_{0.98}MA_{0.02})_{0.95}Pb(I_{0.98}Br_{0.02})_3$/PDI/PCBM/BCP/Ag	23.19		[33]
FTO/Ph-4PACz/$Cs_{0.05}(FA_{0.98}MA_{0.02})_{0.95}Pb(I_{0.98}Br_{0.02})_3$/PDI/PCBM/BCP/Ag	25.01	w/o encapsulation, 85 °C, N_2, keep 72.2% after 1000 h; 65 °C, N_2, MPP tracking, keep ~83% after 1000 h	
FTO/Ph-4PACz/Al_2O_3/$Cs_{0.05}(FA_{0.98}MA_{0.02})_{0.95}Pb(I_{0.98}Br_{0.02})_3$/PDI/PCBM/BCP/Ag	25.60 (24.48 certified, 1 cm^2)	w/o encapsulation, 85 °C, N_2, keep 90.5% after 1000 h; 65 °C, N_2, MPP tracking, keep 91.7% after 1000 h	
ITO/2PACz/$Cs_{0.05}FA_{0.85}MA_{0.1}Pb(I_{0.97}Br_{0.03})_3$/LiF/$C_{60}$/BCP/Ag	24.11	w/o encapsulation, N_2, ~45 °C, MPP tracking, keep 70% after 1000 h	[34]
ITO/I-2PACz/$Cs_{0.05}FA_{0.85}MA_{0.1}Pb(I_{0.97}Br_{0.03})_3$/LiF/$C_{60}$/BCP/Ag	25.39	w/o encapsulation, N_2, ~45 °C, MPP tracking, keep 96% after 1000 h	
ITO/Me-4PACz/$Cs_{0.05}FA_{0.85}MA_{0.1}PbI_3$/$PC_{61}BM$/$C_{60}$/BCP/Cu	24.14	ISOS-L1: w/o encapsulation, N_2, 50 ± 10 °C, MPP tracking, keep 74.07% after 3100 h	[42]
ITO/Me-Ph*p*PACz/$Cs_{0.05}FA_{0.85}MA_{0.1}PbI_3$/$PC_{61}BM$/$C_{60}$/BCP/Cu	26.12 (certified)	ISOS-L1: w/o encapsulation, N_2, 50 ± 10 °C, MPP tracking, keep 98.70% after 3100 h	
ITO/MPA-CPA/$Cs_{0.05}(MA_{0.05}FA_{0.95})_{0.95}Pb(I_{0.95}Br_{0.05})_3$/$C_{60}$/BCP/Ag	25.40 (certified) 22.00 (9.66 cm^2)	encapsulated, 30–40% humidity, ~45 °C, MPP tracking, keep >90% after 2000 h; 85 °C, 85% humidity, keep >95% after 500 h	[51]
ITO/ALD ITO/MeO-2PACz/$Cs_{0.05}(FA_{0.95}MA_{0.05})_{0.95}Pb(I_{0.95}Br_{0.05})_3$/$C_{60}$/ZnO/Au	24.0	ISOS-D-3: encapsulated, 85 °C, 85% humidity, dark, keep 95.0% after 1000 h; ISOS-L-2: encapsulated, 85 °C, 85% humidity, MPP tracking, keep 93.5% after 1200 h	[66]
ITO/ALD ITO/DC-TMPS/$Cs_{0.05}(FA_{0.95}MA_{0.05})_{0.95}Pb(I_{0.95}Br_{0.05})_3$/$C_{60}$/ZnO/Au	24.8 (24.6 certified)	ISOS-D-3: encapsulated, 85 °C, 85% humidity, dark, keep 98.9% after 1000 h; ISOS-L-2: encapsulated, 85 °C, 85% humidity, MPP tracking, keep 98.2% after 1200 h	

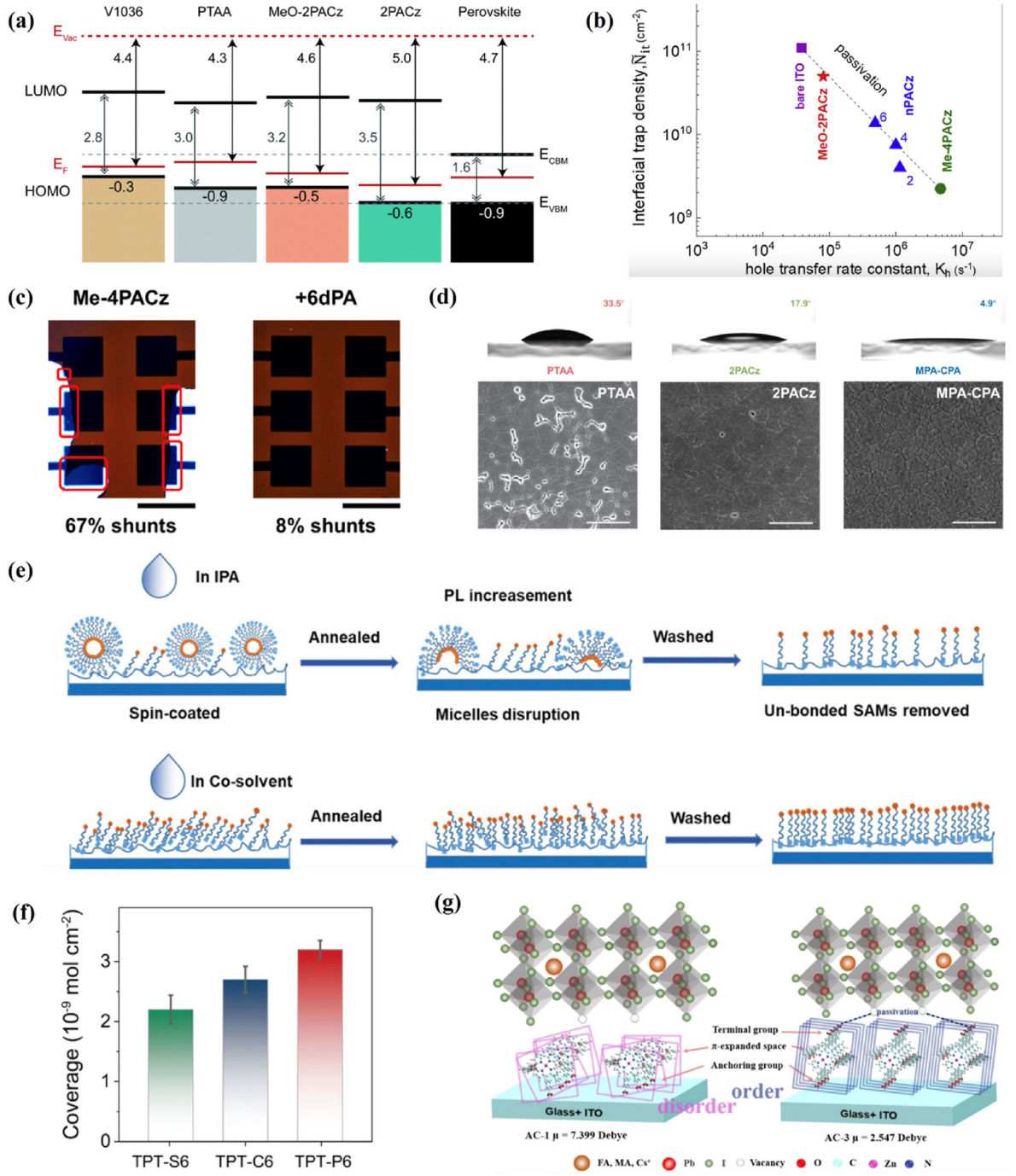

Fig. 4. Several factors should be considered to grow high-quality SAMs on ITO, including energy alignment, carrier extraction, wettability, coverage and SAM-perovskite interactions. (a) Schematic representation of the band edge positions of PVSCs with different SAMs. Reproduced from Ref. [28] with permission from the Royal Society of Chemistry. (b) Hole transfer rate constants versus interfacial trap density. The numbers 2, 4, and 6 denote the chain length in the nPACz series. Reproduced from Ref. [30] with permission from the Elsevier Inc. (c) Optical images of the representative PVSCs with Me-4PACz (left) and Me-4PACz+6dPA selective contact layer. Highlighted in red are the active cell areas not covered by perovskite film. Scale bar = 5 mm. Reproduced from Ref. [54] with permission from the American Chemical Society. (d) Contact angles of the perovskite precursor solution on different HTLs and the top-view SEM images of the bottom surface of perovskites deposited on different HTLs. Scale bars, 1 μm. Reprinted with permission from Ref. [51]. Copyright 2023, The American Association for the Advancement of Science. (e) Schematic diagram for evolution of SAMs configuration adjustment deposited from IPA or co-solvent. Reprinted with permission from Ref. [82]. Copyright 2023, Wiley-VCH GmbH. (f) The coverage of TPT-S6, TPT-C6 and TPT-P6 on ITO substrates. Reprinted with permission from Ref. [47]. Copyright 2021, Wiley-VCH GmbH. (g) Schematic of the SAMs with two carboxyl groups which can anchor to the ITO surface and passivate defects on the perovskite surface. Reprinted with permission from Ref. [75]. Copyright 2023, Wiley-VCH GmbH.

others reported that the perovskite morphology will not be affected by the substrate with different hydrophobicity because the crystallization by one-step solution processes is initiated at the top surface [28,29,47,48,51,84,94]. On the other hand, Zhang et al. [51] found that the hydrophobic surface of the modified ITO may lead to poor buried perovskite-substrate interface with voids, and thus they synthesized an amphiphilic SAM molecule [(2-(4-(bis(4-methoxyphenyl)amino) phenyl)-1-cyanovinyl)phosphonic acid (MPA-CPA) which shows much

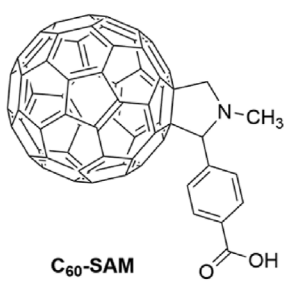

C_{60}-SAM

CN-C_{60}-MPBA

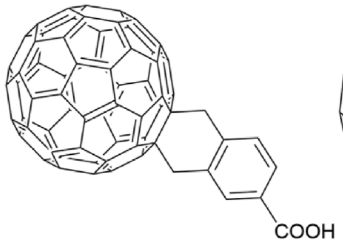

C_{60}-HNA

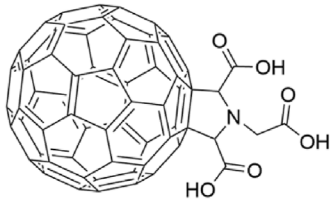

CPTA

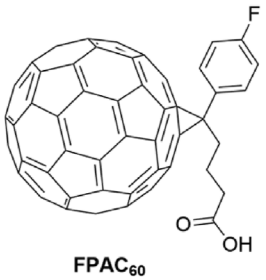

$FPAC_{60}$

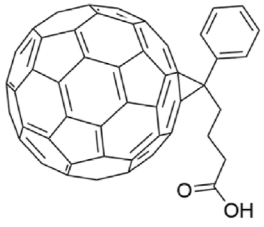

PCBA

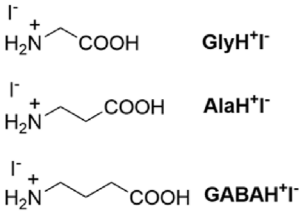

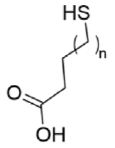

HOOC-$(CH_2)_2$-SH, n = 0
HOOC-$(CH_2)_6$-SH, n = 4
HOOC-$(CH_2)_{11}$-SH, n = 9

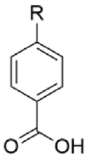

HOOC-Ph-SH, R = SH
PABA, R = NH_2
BA, R = H
CBA, R = CN
ABA, R = NH_2r
BA-CF_3, R = CF_3
BA-CH_3, R = CH_3
BBA, R = Br

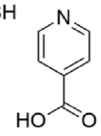

PA

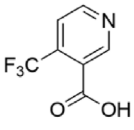

NA-CF_3

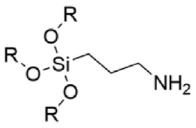

APTMS, R = CH_3
APTES, R = CH_2CH_3

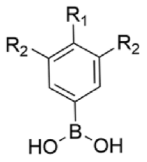

1-OMe, R_1 = OCH_3, R_2, R_3= H
2-OMe, R_1 = H, R_2, R_3 = OCH_3
3-OMe, R_1, R_2, R_3 = OCH_3

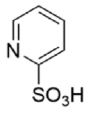

2-PA

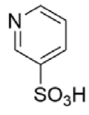

3-PA

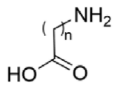

C_3-SAM, n = 2
glycine, n = 1

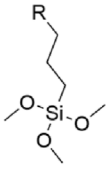

γ-MPTS, R = SH
H-SAM, R = H
I-SAM, R = I
-C3-Cl, R = Cl
EDPTMS, R = $NH(CH_2)_2NH_2$

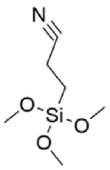

-C3≡N

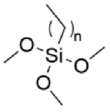

C0, R = 0
C2, R = 2
C3, R = 3

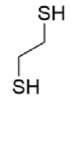

EDT

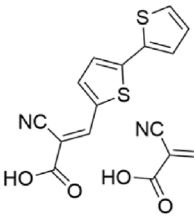

T2CA

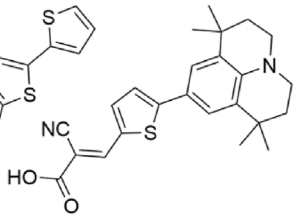

JTCA

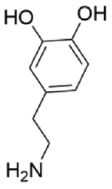

Dopamine

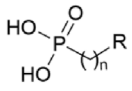

IMPA, n = 1, R = I
IBPA, n = 4, R = I
IHPA, n = 6, R = 1
BPA, n = 3, R = CH_3
APPA, n = 3, R = NH_2
TFBPA, n = 3, R = CF_3
EPA, n = 1, R = CH_3

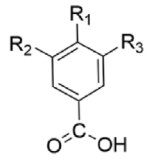

MBA, R_1 = OCH_3, R_2, R_3 = H
DMBA, R_1, R_2 = OCH_3, R_3 = H
TMBA, R_1 ,R_2, R_3 = OCH_3

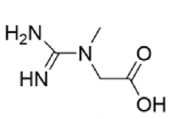

creatine

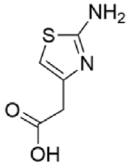

ATAA

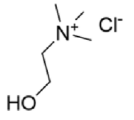

choline chloride

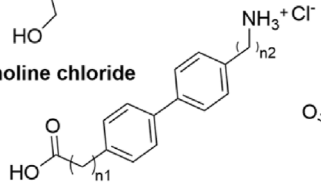

HO_2C-PP-NH_3Cl, n_1 = 0, n_2 = 0
HO_2C-PP-CH_2NH_3Cl, n_1 = 0, n_2 = 1
HO_2C-CH_2-PP-CH_2NH_3Cl, n_1 =1, n_2 = 1

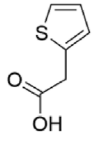

2-TA

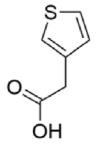

3-TA

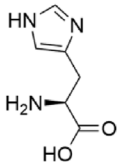

***L*-histidine**

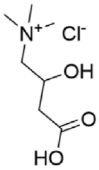

L-ch

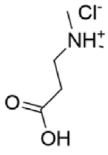

DPAH

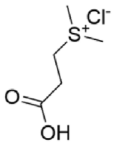

CDSC

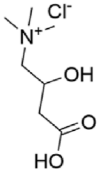

DL-carnitine hydrochloride

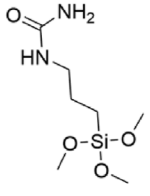

TMPU

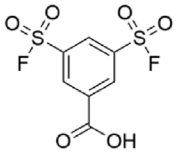

FBA

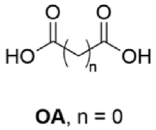

OA, n = 0
PA, n = 1
SA, n =2

(caption on next page)

Fig. 5. Chemical structures of SAM molecules used to modify metal oxide ETLs in n-i-p PVSCs: C_{60}-SAM [105,106], fullerene derivatives [107], C_{60} pyrrolidine tris-acid (CPTA) [6,6,108]-4-fluorophenyl-C_{61}-butyric acid ($FPAC_{60}$) [109], PCBA [129], β-glycine HI salt ($GlyH^+I^-$), alanine HI salt ($AlaH^+I^-$), and γ-amino butyric acid HI salt ($GABAH^+I^-$) [116], HOOC-R-SH [117], 4-aminobenzoic acid (PABA) [119], benzoic acid (BA), 4-cyanobenzoic acid (CBA), 4-aminobenzoic acid (ABA) and 4-pyridinecarboxylic acid (PA) [136], 4-(trifluoromethyl) benzoic acid (BA-CF_3), p-toluic acid (BA-CH_3) and 4-methylnicotinic acid (NA-CF_3) [143], 4-bromobenzonic acid (BBA) [154], aminopropyltrimethoxysilane (APTMS) [118], 3-aminopropyltriethoxysilane (APTES) [137], 4-methoxyphenylboronic acid (1-OMe), 3,5-methoxyphenylboronic acid (2-OMe) and 3,4,5-methoxyphenylboronic acid (3-OMe) [120], 2-pyridinesulfonic acid (2-PA) and 3-pyridinesulfonic acid (3-PA) [121], 3-aminopropanioc acid (C_3-SAM) [128], glycine [139], γ-mercaptopropyltrimethoxysilane (γ-MPTS) [122], propyltrimethoxysilane (H-SAM) and 3-iodopropyl trimethoxysilane (I-SAM) [142], 3-chloropropyl trimethoxysilane (-C3-Cl) and 3-(triehtoxysilyl)propionitrile (-C3≡N) [151], *N*-[3-(trimethoxysilyl) propyl]ethylenediamine (EDPTMS) [123], methyltrimethoxysilane (C0), propyltrimethoxysilane (C2) and butyltrimethoxysilane (C3) [126], 1,2-ethanedithiol (EDT) [130], T2CA and JTCA [131], dopamine (DA) [138], iodomethylphosphonic acid (IMPA), 4-iodobutylphosphonic acid (IBPA), and 6-iodohexylphosphonic acid (IHPA), *n*-butylphosphonic acid (BPA), 3-aminopropylphosphonic acid (APPA), and 4,4,4-trifluorobutylphosphonic acid (TFBPA) [125], ethylphosphonic acid (EPA) [154], 4-methoxybenzoic acid (MBA), 3,4-dimethoxybenzoic acid (DMBA), and 3,4,5-trimethoxybenzoic acid (TMBA) [132], creatine [140], (2-aminothiazole-4-yl)acetic acid (ATAA) [133], choline chloride [141], HO_2C-PP-NH_3Cl, HO_2C-PP-CH_2-NH_3Cl and HO_2C-CH_2-PP-CH_2-NH_3Cl [134], 2-thiophene acetic acid (2-TA) and 3-thiophene acetic acid (3-TA) [135], L-carnitine hydrochloride (L-ch) [144], L-histidine (L-His) [145], (3-dimethylamino propionic acid hydrochloride (DPAH) and ((2-carboxyethyl) dimethyl sulfonium chloride (CDSC) [146], DL-carnitine hydrochloride [147], 1-[3-(trimethoxysilyl)propyl]urea (TMPU) [148], 3,5-bis(fluorosulfonyl)benzoicacid (FBA) [149], oxalic acid (OA), propanedioic acid (PA) and succinic acid (SA) [150].

enhanced hydrophilicity compared to 2PACz, arising from the polar and electron-withdrawing cyano group adjacent to the phosphonic acid. They further used a bilayer stack which consists of a chemically anchored SAM and an unabsorbed, disordered overlayer to deposit perovskite films. The bilayer stack exhibits superwetting characteristics with a small contact angle (~5°), thus a compact and homogeneous morphology without voids could be achieved at the bottom surface (Fig. 4d). Due to the minimized defects at the buried interface, the p-i-n PVSCs achieve a certified PCE of 25.4%.

2.3. Coverage

A dense and compact monolayer is critical for high performance and high stability of devices because it can minimize the direct contact between active layer and electrode. The above discussed co-SAM strategy was also demonstrated as an efficient way to achieve a dense monolayer. Kapil et al. [52] found that the co-absorption of 2PACz and methyl phosphonic acid (MPA) on ITO could lead to a high performance Sn-Pb PVSC due to the higher SAM packing density and enhanced passivation at the interface. Deng et al. [46] synthesized a carbazole-based hole--selective SAM molecule, ((2,7-dimethoxy-9H-carbazol-9-yl) methyl) phosphonic acid (DC-PA) with increased molecular dipole compared to MeO-2PACz which ensures good energy level alignment with the VBM of the perovskite, while an alkyl ammonium SAM, 6-(iodo-λ^5-azanyl) hexanoic acid (IAHA) was used as the second component in the hole-selective SAM matrix to improve the coverage of monolayer and simultaneously passivate the perovskite on top. Zheng et al. [45] demonstrated that the (aminomethyl)phosphonic acid (AMP) in the precursor solution could spontaneously sinks and anchors to the buried interface to fill the voids of SAM for dense HTL. Mishima et al. [95] found that the surface coverage of 2PACz is larger than that of MeO-2PACz due to the steric effect, and the mixture of 2PACz and MeO-2PACz could achieve the highest surface coverage and thus the best device performance. Wu et al. [96] used the hydrofluoric acid and the subsequent UV-ozone treatment to reconstruct the ITO surface by selectively removing the undesired terminal hydroxyl and hydrolysis product. This can significantly increase the ITO surface activity and area, thus facilitating the adsorption of high-density SAMs. Hu et al. [17] found that benzylphosphonic acid (BnPA)/pentafluorobenzylphosphonic acid (F_5BnPA) mixture could form an compact and ordered SAM on ITO due to the strong arene-perfluoroarene interaction, thus significant improving the stability of OSCs, but this strategy has not been applied in PVSCs. It's noticed that SAMs with short linkers have difficulty forming a dense monolayer because of strong steric hindrance, thus extension of the length of conjugation linker always results in improved device performance [58]. It was also demonstrated that the hydrogen bonding between SAM molecules may induce the self-aggregation which leads to a rough surface and thus poor device performance [59].

Introducing electron-donating or electron-withdrawing groups at terminal or near anchoring groups to tune the molecular dipoles of the SAM molecules are widely used to optimize the energy level alignment at the interfaces [33,38,39,48,55,60–62,64]. However, this strategy may induce steric hindrance which destroys their capabilities in forming ordered and compact SAMs [21,63]. Jiang et al. [35] thus synthesized two carbazole-based SAMs, CbzPh and CbzNaph, with increased dipole moment and π-π interactions through asymmetric and helical π-expansion of carbazole, respectively. The compact π-π stacking facilitates the formation of the densest assembly, achieving a champion PCE of 24.1% for CbzNaph-based p-i-n PVSCs with improved stability.

The amphiphilic nature of SAM molecules will lead to the formation of micelles in the commonly used alcoholic processing solvents, which introduces an extra energetic barrier to disassemble the micelles during the binding on the substrate, limiting the formation of a compact SAM. Liu et al. [82] thus developed a co-solvent strategy to disassemble the micelles of carbazole-based SAM molecules in the processing solution, effectively enhancing the reactivity of the phosphonic acid anchoring group to allow densely packed SAMs on ITO (Fig. 4e). Park et al. [65] also found that the cluster formation during phosphonic acid adsorption leads to incomplete SAM coverage by molecular dynamics simulations. They thus developed a co-adsorbent strategy that disassembles high-order clusters by introducing 3-mercaptopropionic acid (3-MPA) into 2PACz solution, homogenizing the distribution of phosphonic acid molecules. Tang et al. [66] found that the hydrophilic OH groups weakly bonded to ITO and the SAM anchored to these unstable sites can be desorbed by strong polar perovskite solvents. They thus prepared an additional ITO layer by atomic layer deposition (ALD) with a fully covalent OH-covered surface to reinforce the anchoring sites of SAM. Furthermore, they synthesized (3,6-dimethoxy-9H-carbazol-9-yl)trimethoxyphenylsilane (DC-TMPS) with a trimethoxysilane group which shows high binding energy with the chemisorbed OH surface through tridentate anchors, as opposed to the more commonly used SAM with phosphonic acid groups with bidentate anchors. The corresponding p-i-n PVSCs maintained 98% of their PCE after operating at maximum power point (MPP) tracking at 85 °C for 1200 h. Phung et al. [97] also demonstrated that plasma-assisted ALD processed NiO could improve the coverage of MeO-2PACz compared to that on bare ITO.

In additions to phosphonic acids, carboxylic acids [25,58,59,61,63,64,67–79], boronic acids [80,81], sulfonic acid [47], cyano group [72], silane [23,66], hydroxy group [24] have also been used to modify ITO. The anchoring group can remarkably affect the adsorption dynamics, loading density, and binding strength of the SAM molecules on substrates and subsequently determine the device performance and stability. Li et al. [47] synthesized a series of phenothiazine-based SAM molecules with various anchoring groups, -SO_3H (TPT-S6), -COOH (TPT-C6), and -PO_3H_2 (TPT-P6), and found that TPT-P6 is more easily and faster anchored onto ITO with a higher loading amount than TPT-C6 and

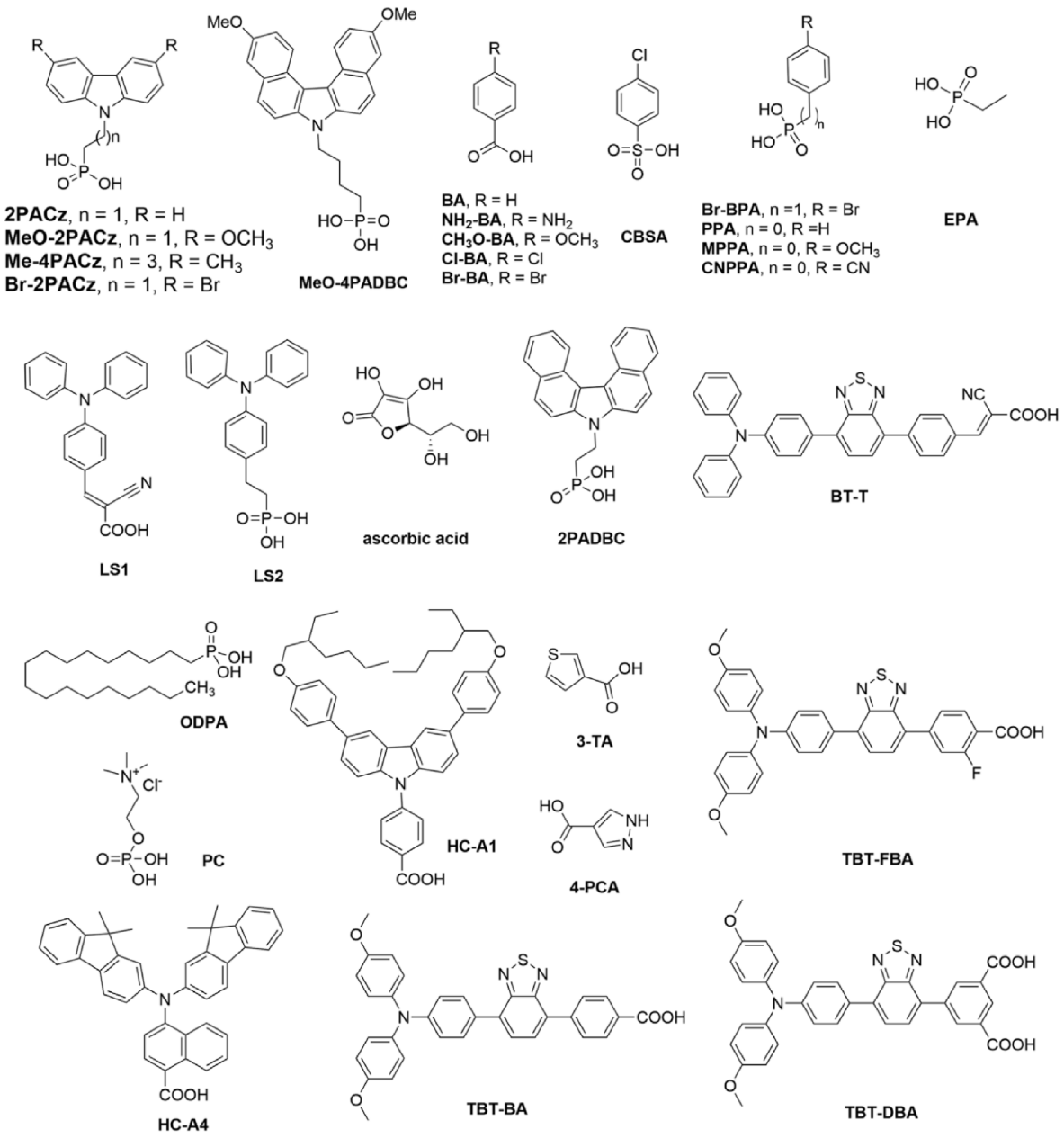

Fig. 6. Chemical structures of SAM molecules used to modify metal oxide HTLs in p-i-n PVSCs: 2PACz and MeO-2PACz [158], MeO-4PADBC [162], Me-4PACz [159], Br-2PACz [165], *para*-substituted benzoic acid (R-BA) [152], *p*-chlorobenzenesulfonic acid (CBSA) [157], 4-bromobenzylphosphonic acid (Br-BPA) [153], phenylphosphonic acid (PPA), 4-methoxyphenylphosphonic acid (MPPA), and 4-cyanophenylphosphonic acid (CNPPA) [155], ethylphosphonic acid (EPA) [154], 2-cyano-3-(4-(diphenylamino) phenyl) acrylic acid (LS1) [156], LS2 [160], ascorbic acid (AA) [161], 2PADBC [170], 2-cyano-3-(4-(7-(4-(diphenylamino)phenyl)benzo[*c*] [1,2,5]thiadiazol-4-yl)phenyl)acrylic acid (BT-T) [163], octadecylphosphonic acid (ODPA) [164], PC [166], HC-A1 and HC-A4 [167], 3-thenoic acid (3-TA) and 4-pyrazolecarboxylic acid (4-PCA) [168], TBT-BA, TBT-FBA and TBT-DBA [169].

TPT-S6, thus leading to improved coverage of the monolayers (Fig. 4f). Furthermore, higher built-in potential which facilitates carrier collection and suppressed interfacial non-radiative recombination for TPT-P6-based devices were also demonstrated, thus higher PCEs were achieved. The device stability is also highly related to the anchoring group, 90% of the initial PCE was kept after three months storage in air with a humidity of 30% for TPT-P6-based device. However, later they found that the strong phosphonic acidic anchors is detrimental to device stability, thus MTPA-BA with acidity-weakened boric acid was synthesized. The corresponding devices show improved stability which retained 90% of their PCE after 2400 h of storage (ISOS-D-1) or 400 h of operation (ISOS-L-1), which are 5-fold higher than those of phosphonic acid SAM-based devices [81].

2.4. Linkers

Most of the reported well-established PACz series SAM molecules are with an alkyl linker which may suffer charge-transport issue. Ren et al. [43] found that increasing the concentration of Me-4PACz from 1 to 3 mg mL^{-1} causes the PCE to dramatically drop from 21.9% to 11.6%. The polymeric SAM molecules, Poly-4PACz, exhibit high conductance and consequently demonstrate good tolerance to layer thickness. Zhang et al. [58] synthesized a series of SAM molecules of cyanoacetic acids with benzene ring as conjugated linkers and demonstrated that the conjugated structure could improve the charge-transport. The SAM molecules also show higher intrinsic photostability of molecular structures and the solution stocks than MeO-2PACz. Afraj et al. [72] synthesized

Table 2
A selected summary of the device structures, photovoltaic parameters and stabilities of PVSCs based on SAM modified CTLs.

Device Structure	PCE [%]	Stability	Ref
ITO/ZnO/$MAPbI_3$/spiro-OMeTAD/MoO_3/Ag	11.96		[128]
ITO/ZnO/C_3-SAM/$MAPbI_3$/spiro-OMeTAD/MoO_3/Ag	15.67		
ITO/SnO_2/$Cs_{0.05}(FA_{0.85}MA_{0.15})_{0.95}Pb(I_{0.85}Br_{0.15})_3$/spiro-OMeTAD/Au	20.15	w/o encapsulation, N_2, MPP tracking, T_{80} = ~692 h	[142]
ITO/SnO_2/H-SAM/ $Cs_{0.05}(FA_{0.85}MA_{0.15})_{0.95}Pb(I_{0.85}Br_{0.15})_3$/spiro-OMeTAD/Au	20.19	w/o encapsulation, N_2, MPP tracking, T_{80} = ~714 h	
ITO/SnO_2/I-SAM/$Cs_{0.05}(FA_{0.85}MA_{0.15})_{0.95}Pb(I_{0.85}Br_{0.15})_3$/spiro-OMeTAD/Au	21.44	w/o encapsulation, N_2, MPP tracking, T_{80} = ~3921 h	
FTO/SnO_2/$(FAPbI_3)_{0.992}(MAPbBr_3)_{0.008}$/spiro-OMeTAD/Au	23.7	encapsulated, 25 °C, 20–40% humidity, MPP tracking, keep 50% after 310 h	[151]
FTO/SnO_2/-C3-Cl/$(FAPbI_3)_{0.992}(MAPbBr_3)_{0.008}$/spiro-OMeTAD/Au	24.7	encapsulated, 25 °C, 20–40% humidity, MPP tracking, keep 77% after 500 h	
FTO/SnO_2/-C3-C ≡ N/$(FAPbI_3)_{0.992}(MAPbBr_3)_{0.008}$/spiro-OMeTAD/Au	25.3	encapsulated, 25 °C, 20–40% humidity, MPP tracking, keep 97% after 1000 h	
FTO/NiO_x/$FAPbI_3$/$PC_{61}BM$/SnO_2/Cu	22.2		[159]
FTO/NiO_x/Me-4PACz/$FAPbI_3$/$PC_{61}BM$/SnO_2/Cu	25.5 (25.2 certified)	50 °C, MPP tracking, keep 85.4% after 1000 h; 85 °C, keep 85.1% after 500 h	
	21 (14.65 cm^2)	50 °C, MPP tracking, keep 90% after 400 h	
ITO/NiO_x/MeO-4PADBC/ $Cs_{0.05}FA_{0.8}MA_{0.15}Pb(I_{0.76}Br_{0.24})_3$/$C_{60}$/BCP/Ag	25.6 (certified)	ISOS-L-2I: encapsulated, 65 °C, MPP tracking, keep 90% after 1200 h; encapsulated, 85 °C, MPP tracking, keep 74% after 1200 h	[162]
ITO/NiO_x/$Cs_{0.04}(FA_{0.96}MA_{0.04})_{0.96}Pb(I_{0.96}Br_{0.04})_3$/PCBM/BCP/Ag	20.8	w/o encapsulation, N_2, 60 °C, keep 41.2% after ~2000 h; w/o encapsulation, N_2, 85 °C, keep 19.6% after 150 h; ISOS-L-1: 50 ± 5% humidity, keep 61.9% after ~35 h	[169]
ITO/NiO_x/TBT-BA/ $Cs_{0.04}(FA_{0.96}MA_{0.04})_{0.96}Pb(I_{0.96}Br_{0.04})_3$/PCBM/BCP/Ag	24.8	w/o encapsulation, N_2, 60 °C, keep 88.7% after 2635 h; w/o encapsulation, N_2, 85 °C, keep 85.8% after 200 h; ISOS-L-1: 50 ± 5% humidity, keep 81.2% after 240 h	
ITO/NiO_x/TBT-FBA/ $Cs_{0.04}(FA_{0.96}MA_{0.04})_{0.96}Pb(I_{0.96}Br_{0.04})_3$/PCBM/BCP/Ag	24.0	w/o encapsulation, N_2, 60 °C, keep 82.4% after 2635 h; w/o encapsulation, N_2, 85 °C, keep 80.1% after 200 h	
ITO/NiO_x/TBT-DBA/ $Cs_{0.04}(FA_{0.96}MA_{0.04})_{0.96}Pb(I_{0.96}Br_{0.04})_3$/PCBM/BCP/Ag	23.1	w/o encapsulation, N_2, 60 °C, keep 83.2% after 2635 h; w/o encapsulation, N_2, 85 °C, keep 72.5% after 200 h	

quinoxaline-based SAM molecules with benzene or thiophene as conjugated linker for tin-based PVSCs. The device based on TQxD with thiophene linker as SAM showed a PCE of 8.3% based on $FASnI_3$ which outperforms the device based on MeO-2PACz (6.5%), and the device also showed excellent stability, retaining ~90% of the initial PCE after 1600 h. Hung et al. [75] synthesized a series of hole-selective SAMs based on Zn^{II} porphyrin, namely AC-1, AC-3, and AC-5, in which the π-conjugated porphyrin core serves as an ideal conduit for efficient charge carrier transport. The dual carboxylic acid groups in AC-3 and AC-5 facilitate effective anchoring to the ITO surface while passivating the buried interface of perovskites (Fig. 4g). As a result, PVSCs with a PCE of 23.19% and excellent device stability were achieved. Recently, Li et al. [41] and Qu et al. [42] synthesized novel fully aromatic carbazole-based SAMs (4-(3,6-dimethoxy-9H-carbazol-9-yl)phenyl)phosphonic acid (MeO-Ph-PACz) and [4-(3,6-dimethyl-9H-carbazol-9-yl)phenyl]phosphonic acid (Me-Ph*p*PACz) respectively by replacing the flexible alkyl linker in MeO-2PACz and Me-4PACz with a rigid, planar, and conjugated phenylene linker. Due to the larger dipole moment, enhanced hole extraction kinetics, and improved hole transport characteristics of MeO-PhPACz and Me-Ph*p*PACz, the corresponding devices showed improved PCEs compared to those based on the classic MeO-2PACz and Me-4PACz. The Me-Ph*p*PACz-derived PVSCs exhibit an unprecedented PCE of 26.17% (26.12% certified) with an extremely high FF of 86.79% and exceptional long-term stability [42].

Hole extraction is expected to be more efficient when the π-cores are oriented face-on with respect to the surfaces. Truong et al. [56] thus used multiple phosphonic acid anchoring groups to control the molecular orientation of a series of triazatruxene derivatives chemisorbed on FTO. They found that multipodal derivatives align face-on to the electrode surface, while the monopodal counterpart adopts a more tilted configuration. The face-on orientation was found to facilitate hole extraction, leading to p-i-n PVSCs with enhanced stability and high PCE of 23.0%. To increase the hydrophilicity of the SAM modified electrode, they further synthesized a multipodal molecule with a non-planar π-conjugated core, some anchoring groups would be forced to point upward while not binding to the FTO surface. These top-facing functional groups would lead to a more hydrophilic surface and improve wettability [57].

2.5. Terminal groups

The interaction of the SAM molecules, usually by the terminal groups of the SAMs, with the perovskite, is also crucial for the device performance and stability and should be carefully designed. Ashouri et al. [29] and Levine et al. [30] demonstrated the advantages of the methyl substitution with respect to both passivation and hole extraction in PACz derivatives. Deng et al. [46] used an alkyl iodine-terminated ammonium SAM molecule (IAHA) as the second component in the hole-selective SAM matrix to passivate the perovskite on top. Ullah et al. [48,49] investigated the effects of terminal group heteroatoms (O, S, Se) of phosphonic acids-based SAMs on device performance. The stronger interaction between Br-2EPSe and perovskite reduces interfacial trap density and thus a higher PCE of 22.73% was achieved for Br-2EPSe based p-i-n PVSCs compared to 21.63% and 21.02% for Br-2EPT and Br-2EPO based PVSCs. The unencapsulated PVSC with Br-2EPSe also showed excellent stability, retaining up to ~96% of its initial PCE after an MPP tracking of >500 h under ambient conditions. Almasabi et al. [98] demonstrated that the stronger binding of MeO-2PACz than PTAA towards $FAPbI_3$ could result in enhanced mechanical adhesion of the single-crystal films on the substrate, enabling the fabrication of PVSCs with substantially enhanced operational stability. Dai et al. [34] demonstrated that an iodine-terminated 2PACz (I-2PACz) increases the interfacial mechanical adhesion dramatically (2.6-fold) and contributes to the improved interfacial morphology, photocarrier transport, and operational stability. The corresponding PVSCs show a high PCE of 25.39%. Additionally, the enhanced adhesion suppresses nucleation and propagation of pores/cracks during operation, resulting in the retention of 96% of the initial PCE after 1000 h of MPP tracking. Jiang et al. [44] designed Cbz2S and Cbz2SMe with cyclic disulfide or two flanking thiomethyls by modifying the 4,5-position of carbazole. Cbz2S with more-exposed sulfur atoms exhibited inferior device performance due to excessive reactivity, leading to an overpopulation of PbI_2 crystallites at the buried perovskite interface. In contrast, the screening effect from the methyl groups of Cbz2SMe optimized SAM reactivity, exquisitely integrating buried interface passivation and hole selection together. Consequently, Cbz2SMe-based PVSCs achieve a PCE of 24.42% with excellent

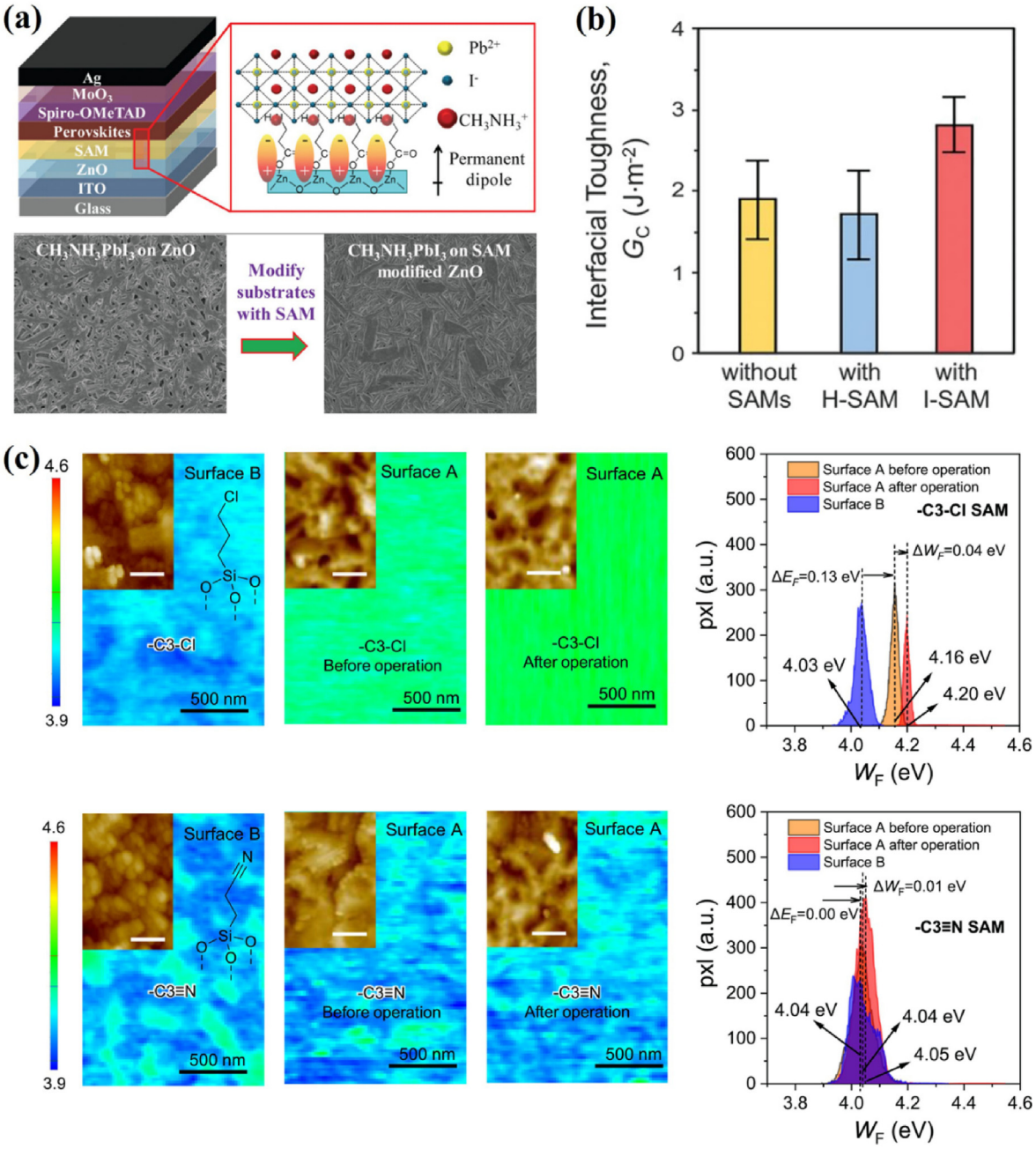

Fig. 7. The SAM modification at metal oxide CTLs could optimize perovskite morphology, increase interfacial toughness and stabilize interface. (a) Schematic diagram of PVSC device structure, SAM induced permanent dipole formation, and involvement of the SAM in the crystalline structure of perovskite crystals. SEM images of $MAPbI_3$ perovskites on bare ZnO and ZnO/C_3-SAM. Reprinted with permission from Ref. [128]. Copyright 2015, American Chemical Society. (b) Toughness of SnO_2/perovskite interface without SAMs and ones with H-SAM or I-SAM. The histograms and error bars represent average and standard deviation, respectively, of 12 specimens each. Reprinted from Ref. [142] with permission. Copyright 2021, The American Association for the Advancement of Science. (c) Kelvin probe force microscope (KPFM) images and WF distributions obtained from the KPFM data of surface B, and surface A before and after operation of PVSCs with -C3-Cl and -C3≡N SAMs. The "surface A″ and "surface B″ are the bottom of the perovskite film and the upper surface of the SnO_2 film respectively. Reprinted from Ref. [151] with permission. Copyright 2024, Elsevier Inc.

stability. Recently, an increasing number of new SAM molecules with terminal groups capable of passivating the buried interface of perovskite films, such as CbzBF, CbzBT [40], TDPA-Cl [50], MeO-BTBT [53], were synthesized for PVSCs.

In addition to the terminal groups, the anchoring groups of the SAM molecules could also be used to construct interfaces with desired properties during perovskite film deposition. For example, Azmi et al. [99] utilized the phosphonic acid group of the 2PACz to react with 4-hydroxybenzylamine (HBzA), enabling the formation of 2D ligands that are resilient to subsequent processing through the creation of an ionic bond. With this, p-i-n PVSCs with double-side 2D/3D heterojunctions were successfully constructed with a PCE of 25.6% (certified 25.0%), retaining 95% of their initial PCE after 1000 h of operation at 85 °C in air.

2.6. Application in tandem and large-area solar cells

Due to the advantages of energy level tunability, conformal coverage and low temperature processing, SAMs are promising in flexible [64] and tandem solar cells [28,29,37,84,95,100,101]. The MeO-2PACz SAM was firstly integrated into a monolithic CIGS/perovskite tandem solar cell by

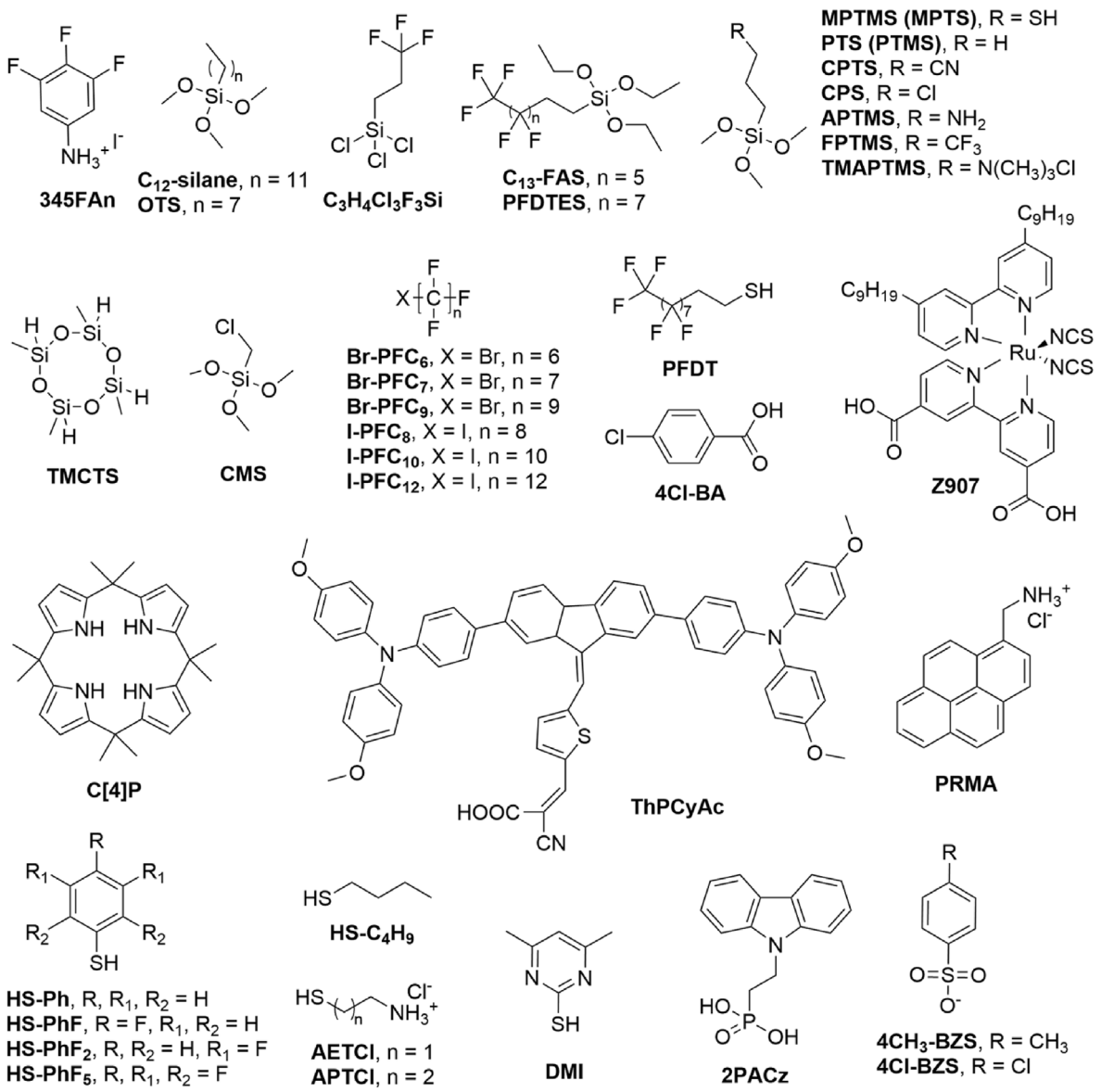

Fig. 8. Chemical structures of SAM molecules used to modify perovskites: 345FAn [178], C_{12}-silane [179], OTS [180], $C_3H_4Cl_3F_3Si$ [181], C_{13}-FAS [182], MPTMS (MPTS) [183], PTS (PTMS) and CPTS [184], CPS and CMS [185], APTMS [186], 2,4,6,8-tetramethylcyclotetrasiloxane (TMCTS), MPTMS, FPTMS, 1*H*,1*H*,2*H*, 2*H*-perfluorodecyltriethoxysilane (PFDTES) and *N*-[3- (trimethoxysilyl)propyl]-*N*,*N*,*N*-trimethylammonium chloride (TMAPTMS) [187], X-PFC_n [188], PFDT [189], 4-chlorobenzoic acid (4Cl-BA) [190], *cis*-diisothiocyanato-(2,2′-bipyridyl-4,4′-dicarboxylic acid)-(2,2′-bipyridyl-4,4′-dinonyl) ruthenium (II) (Z907) [191], C [4]P [192], ThPCyAc [193], PRMA [194], thiols [117], AETCl and APTCl [195], 2-mercaptopyrimidine (DMI) [196], 2PACz [197], [4-methylbenzenesulfonate ($4CH_3$-BZS) and 4Cl-BZS [198].

Ashouri et al. [28], which shows the ability to conformally create a hole-selective layer on a rough surface, and a stabilized, certified PCE of 23.26% with an active area of 1.03 cm^2 was achieved. Later, they utilized Me-4PACz to enable a certified PCE of 29.15% for Si/perovskite tandem solar cell. The tandem solar cell also shows high stability, retaining 95% of its initial efficiency after 300 h of operation in air without encapsulation [29]. Datta et al. [100] used Me-4PACz and 2PACz to minimize the energetic loss at the hole-transporting interface in front WBG subcell in all-perovskite tandem solar cell, and a >23% efficient monolithic all-perovskite tandem solar cell was achieved. Lai et al. [101] used 2PACz as a hole extraction layer to effectively suppress the V_{OC} loss and to enable the growth of high-quality uniform 1.77 eV WBG perovskite absorber on a flexible PEN/ITO. Thus, a maximum efficiency of over 15% with a V_{OC} of 1.29 V for a flexible WBG PVSC was achieved. Two-terminal and four-terminal flexible all-perovskite tandem cells were also successfully fabricated with PCEs of 23.8% and 22.6%, respectively [101]. Later, they further demonstrated a high V_{OC} of 1.31 V in a 1.77-eV WBG PVSC, corresponding to a very low V_{OC} deficit of 0.46 V by integrating (4-(7H-dibenzo[*c*,*g*]carbazol-7-yl)butyl)phosphonic acid (4PADCB, CbzNaph in Ref. [35]). With these WBG perovskite subcells, monolithic all-perovskite tandem solar cells for a PCE of 27.0% (26.4% certified) with an aperture area of 1.044 cm^2 were achieved [37].

SAMs also show great potential as efficient HTLs for upscaling PVSCs and producing large-area perovskite films with high-quality buried interface due to the better and tunable wettability compared to the most widely used HTL PTAA [102,103]. Zeng et al. [102] fabricated MeO-2PACz SAMs and perovskite films by blade-coating, and the perovskite mini-module shows a PCE of 14.13% with an aperture area of 18.0 cm^2. Zhang et al. [51] utilized a superwetting underlayer for perovskite deposition by a bilayer stack of amphiphilic SAM molecule MPA-CPA, thus a PCE of 22.0% was achieved for a spin-coated mini-module with an area of ~10 cm^2. Zheng et al. [90] incorporated SAM

Table 3
A selected summary of the device structures, photovoltaic parameters and stabilities of PVSCs based on SAMs modified perovskites.

Device structure	PCE [%]	Stability	
FTO/2PACz/$Cs_{0.05}MA_{0.05}FA_{0.9}PbI_{2.85}Br_{0.15}$/345FAn/$C_{60}$/BCP/Ag	24.09 (certified)	ISOS-L-3: encapsulated, 85 °C, 50% humidity, T_{85} = ~1560 h	[178]
FTO/c-NiO/perovskite/$PC_{61}BM$/BCP/Ag	20.15	w/o encapsulation, N_2, 85 °C, MPP tracking, keep 46.2% after 500 h; w/o encapsulation, 85 ± 10% humidity, keep ~100% after 500 h	[189]
FTO/c-NiO/PFDT@perovskite/$PC_{61}BM$/BCP/PFDT@Ag	21.79	w/o encapsulation, N_2, 85 °C, MPP tracking, keep 90.1% after 500 h; w/o encapsulation, 85 ± 10% humidity, keep ~35% after 500 h	
ITO/MTPA-BA/$FA_{0.8}Cs_{0.2}PbI_3$/$PC_{61}BM$/C_{60}/BCP/Ag	22.5	ISOS-L-1: 45 °C, N_2, 0% within 200 h; ISOS-D-2: 85 °C, N_2, 0% within 350 h	[192]
ITO/MTPA-BA/$FA_{0.8}Cs_{0.2}PbI_3$/C [4] P/$PC_{61}BM$/C_{60}/BCP/Ag	23.4	ISOS-L-1: 45 °C, N_2, keep 90% after 2000 h; ISOS-D-2: 85 °C, N_2, 90% after 2100 h; 25 ± 5% humidity, MPP tracking, keep 80% after 700 h; 85 °C, dark, keep 89% after 700 h; 85 °C, light, keep 87% after 500 h	
FTO/SnO_2/$Cs_{0.05}FA_{0.85}MA_{0.10}Pb(I_{0.97}Br_{0.03})_3$/spiro-OMeTAD:F4TCNQ/Ag	21.88	w/o encapsulation, 75 ± 5% humidity, 30 ± 5 °C, keep 58% after ~1800 h; w/o encapsulation, N_2, 65 °C, keep 52% after 800 h	[194]
FTO/SnO_2/$Cs_{0.05}FA_{0.85}MA_{0.10}Pb(I_{0.97}Br_{0.03})_3$/PRMA/spiro-OMeTAD:F4TCNQ/Ag	24.03	w/o encapsulation, 75 ± 5% humidity, 30 ± 5 °C, keep 85% after ~1800 h; w/o encapsulation, N_2, 65 °C, keep 81% after 800 h	
FTO/4PADCB/$FA_{0.85}MA_{0.1}Cs_{0.05}PbI_3$/$C_{60}$/BCP/Ag	22.60	w/o encapsulation, N_2, 85 °C, keep 58% after 500 h; N_2, MPP tracking, keep 63% after 500 h	[195]
FTO/4PADCB/$FA_{0.85}MA_{0.1}Cs_{0.05}PbI_3$/2AETCl/$C_{60}$/BCP/Ag	25.00	w/o encapsulation, N_2, 85 °C, keep 82% after 500 h; N_2, MPP tracking, keep 95% after 500 h	
FTO/4PADCB/$FA_{0.85}MA_{0.1}Cs_{0.05}PbI_3$/2APTCl/$C_{60}$/BCP/Ag	24.08		
FTO/2PACz/$Cs_{0.05}FA_{0.85}MA_{0.10}PbI_3$/$C_{60}$/$SnO_x$/Ag	24.0	ISOS-D-2I: 85 °C, keep 89% after 1500 h; ISOS-l-3: encapsulated, 50% humidity, 65 °C, MPP tracking, T_{85} = 1200 h	[198]
FTO/2PACz/$Cs_{0.05}FA_{0.85}MA_{0.10}PbI_3$/4Cl-BZS/$C_{60}$/$SnO_x$/Ag	26.3 (26.15 certified)	ISOS-D-2I: 85 °C, keep 95% after 1500 h; ISOS-l-3: encapsulated, 50% humidity, 65 °C, MPP tracking, T_{95} = 1200 h	

molecules into perovskite precursors when blade-coating which could solve the wetting issue and simplify the device fabrication, and a PCE of 22.5% was achieved for a 1 cm^2 blade-coated device.

3. Modification of metal oxide CTLs by SAMs in PVSCs

Ideal CTLs should efficiently extract photogenerated charge carriers from the perovskites and provide stable interfaces for high stability. The modification of the metal oxide CTLs using SAMs to improve the device performance and stability has been widely applied in OSCs [15,104], and this strategy is also extensively used in PVSCs today after the first reported work of TiO_2 modification with fullerene based SAMs by Jen et al. [105,106], which could improve the device performance with reduced hysteresis [107–109]. TiO_2 is one of the most widely used ETL in n-i-p devices. However, a critical instability in mesoporous TiO_2-sensitized solar cells was reported, arising from light-induced desorption of surface-adsorbed oxygen [110]. ZnO and SnO_2 are other metal oxides explored as alternative ETLs, but ZnO can react easily with perovskites during thermal annealing (>100 °C) due to the proton-transfer reactions at the ZnO/perovskites interface [111], thus SnO_2 appears to be the most promising candidate and can be processed at low temperatures [13,112]. For p-i-n devices, now NiO_x has been demonstrated to be one of the most promising HTLs [113], but the undesired reaction between perovskite and the highly active $Ni^{\geq 3+}$ species, and charge carrier recombination at the NiO_x/perovskite interface limit the device performance and stability [114,115]. The modification of these metal oxide CTLs, TiO_2 [116–127], ZnO [128–135], SnO_2 [136–151], NiO_x [152–169], by SAMs has been demonstrated to be an efficient way to address these discussed issues, and also passivate the surface defects and tune the energy level alignment. Recently, Li et al. [162] improved and stabilized the NiO_x/perovskite interface with modification of (4-(3,11-dimethoxy-7H-dibenzo[*c,g*]carbazol-7-yl)butyl)phosphonic acid (MeO-4PADBC). The resulting PVSCs achieved a certified PCE of 25.6% and maintained >90% of their initial efficiency after continuously operating at 65 °C for 1200 h. The principles of SAM design for metal oxides modification can be referred to the modification of metal oxides in OSCs [15] and the ITO modification in PVSCs as discussed in the above section, thus the discussion will be more briefly in this section.

The chemical structures of the molecules used to modify metal oxide ETLs and HTLs in PVSCs are shown in Figs. 5 and 6, respectively, while the device structures and photovoltaic parameters of PVSCs based on SAM modified metal oxide CTLs are listed in Table 2 and Table S2.

The morphology control is one of the major challenges to achieve high efficiency devices especially in the early stage of the perovskite research. The modification of metal oxide CTLs with SAMs facilitates the crystal growth of perovskite films. Zuo et al. [128] developed a facile but efficient method to modify ZnO with 3-aminopropanioc acid (C_3-SAM) to direct the crystalline evolution and achieve the optimal morphology of $MAPbI_3$ perovskite film with reduced pinholes and trap states density. Furthermore, the WF of the modified cathode was better aligned with the conduction band minimum (CBM) of perovskite for efficient charge extraction, thus the PCEs remarkably increased from 11.96% to 15.67% (Fig. 7a). Later, they applied this strategy into semi-roll-to-roll processing for flexible PVSCs to achieve enhanced performance [171]. Many SAM molecules with an anchoring group to metal oxide CTLs and a functional terminal group such as thiol [117], amnio group [118,119,137] as a growth site of the perovskite crystals are developed later. Yang and Dai et al. [127,142] demonstrated the substantial toughening of the brittle interface between the perovskite film and the underlying metal oxide CTLs using an iodine-terminated silane SAM which acts as a "molecular glue" (Fig. 7b). The device shows enhanced PCE and improved operational stability.

The SAM modification with different terminal groups changes the energy level alignment at the interface which may affect the device performance. Zuo et al. [136] found that the device performance of PVSCs shows an opposite trend to that of the energy level alignment theory which works well in OSCs. The chemical interactions are the predominant factor governing the interfacial optoelectronic properties and thus the performance of PVSCs. Zhang et al. [151] demonstrated that the energy-level alignment at the weak adhesion homojunction interface is critical, as the enhanced ion migration caused by the built-in electric field at this interface may lead to instability (Fig. 7c). Tuning the WF of the homojunction with different terminal groups in the SAM molecules could significantly reduce the built-in electric field, and thus PVSCs with a high PCE and excellent stability were achieved.

The significance of the SAM coverage on ITO surface has been demonstrated and many strategies have been developed to increase the coverage, however this is less investigated on metal oxide CTLs. Cao et al. [166] employed a co-SAM strategy by mixing Me-4PACz and phosphorylcholine chloride (PC) to modify NiO_x surface with improved monolayer coverage and reduced leakage current. Furthermore, the quaternary ammonium ions and Cl^- in PC can fill organic cations and halogen vacancies in the perovskite film to enable defects passivation. Consequently, the Co-SAM modified devices show a PCE of 25.09% with

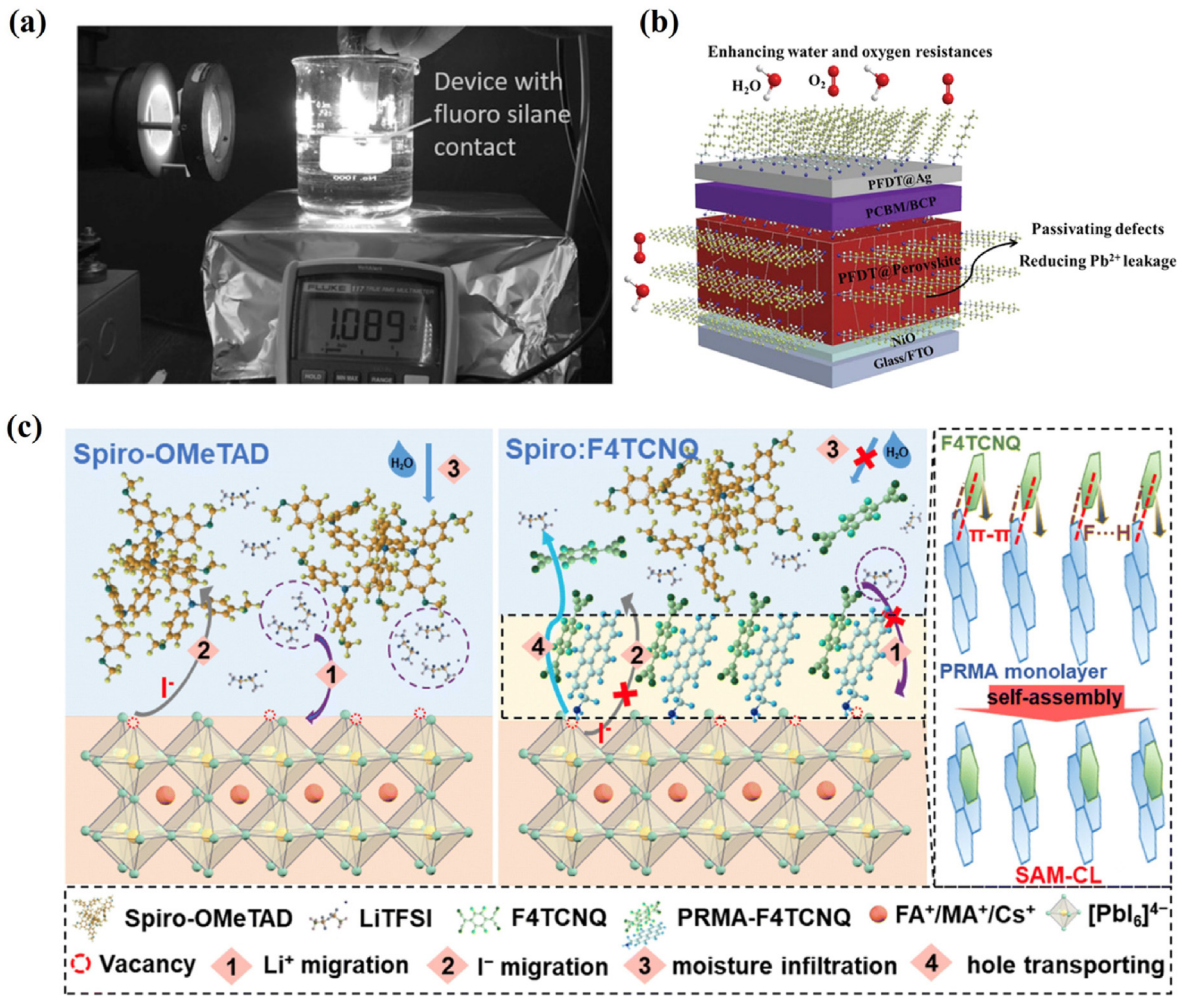

Fig. 9. The SAM modification on perovskite could protect the underneath perovskite films from water, oxygen attacking, and affect charge extraction. (a) A picture showing the PVSC with fluoro-silane layer had a 1.089 V photovoltage output in water. Reprinted from Ref. [181] with permission. Copyright 2016, Wiley-VCH GmbH. (b) Schematic showing the device configuration of PFDT-modified p-i-n PVSC, and the effect on environment-related degradation, defect chemistry and lead leakage issues. Reprinted from Ref. [189] with permission. Copyright 2021, Wiley-VCH GmbH. (c) Schematic illustration of the assembly process and interfacial operating mechanism about SAM-CL. Unmodified device interface has numerous defects and severe water-oxygen erosion occurs, causing Li^+ aggregation and ion migration. The device with SAM-CL has better carrier transport capability, defect passivation, moisture barrier and ion migration inhibition abilities due to an ordered cocrystal structure formed by intermolecular interaction. Reproduced from Ref. [194] with permission, the Royal Society of Chemistry.

excellent device stability with 93% initial efficiency after 1000 h of operation. You et al. [159] modulated the NiO_x nanoparticles solution by adding H_2O_2, improving the dispersion of nanoparticles and surface hydroxyl groups for bonding. The modulated NiO_x surface enables homogeneous Me-4PACz growth which was more favorable for the growth of the perovskite and deposition of uniform large-area films. As a result, the corresponding devices exhibit an efficiency of 25.5% (certified 25.2%), and retain 85.4 and 85.1% of the initial efficiency after 1000 h of operation at 50 °C and 500 h of continuous thermal stress at 85 °C, respectively. Recently, Zhou et al. [169] investigated the coverage of SAMs on NiO_x with a series of methoxy-substituted triphenylamine functionalized benzothiadiazole (TBT) based molecules with benzoic acid, 2-fluorobenzoic acid and isophthalic acids as anchoring groups. TBT-BA with the simplest structure is demonstrated to form the densest SAM on NiO_x, thus the corresponding PVSCs show a high PCE of 24.8% with excellent thermal and operational stability.

4. Modification of perovskites by SAMs in PVSCs

Due to the soft ionic crystal nature of perovskite, defects are inevitable during film processing and are mainly located at grain boundaries and surfaces. They can damage the device performance by acting as traps for photogenerated free carriers and provide primary channels for ion migration and act as initiation sites for moisture, oxygen and light-induced degradation [172,173]. These defective surface layers could be removed by adhesive tapes [174], or a nanosecond pulsed ultraviolet laser [175]. On the other hand, forming thin layers of two-dimensional (2D) perovskites on top of the three-dimensional (3D) perovskite film is the most commonly used strategy to fill the cation/anion vacancies to suppress charge recombination to improve the device performance and stability [176,177]. However, the reactivity of ammonium ligands with 3D perovskites may lead to further penetration into the bulk perovskite film and may contribute to deterioration in device performance [178]. Park et al. [178] found that anilinium could minimize reactivity with perovskite, thus were only detected at the top surface of the perovskite film and no 2D phases were observed. Suppressing ligand intercalation into 3D perovskites could significantly improve interface stability under thermal stress. Finally, a certified PCE of 24.09% for p-i-n PVSCs was achieved with modification of 3,4,5-trifluoroanilinium (345FAn). The encapsulated device shows a 1560-h T_{85} at MPP operating at 85 °C and 50% relative humidity.

SAMs have also been demonstrated as an efficient strategy for

modifying the perovskite surface to suppress interface nonradiative recombination, thereby improving device performance and stability. The structures of reported molecules used to modify perovskite in PVSCs are shown in Fig. 8. The device structures, photovoltaic parameters and stabilities are listed in Table 3 and Table S3.

Among the SAMs, the organosilanes were firstly used to modify perovskites and were the most promising candidates due to their unique cross-linking ability by forming Si–O–Si bonds, which makes a robust layer to protect the underneath perovskite films from water attacking. In 2015, Zhang et al. [179] used dodecyltrimethoxysilane (C_{12}-silane) to modify perovskite to block electron recombination and resist moisture simultaneously. Li et al. [180] used trichloro(octyl)silane (OTS) to effectively eliminate the interfacial defects of $FAPbBr_3$, enabling a champion PCE of 30% under 520 nm monochromatic light irradiation (4.8 mW cm^{-2}). Silanes containing C-F bonds show super-hydrophobicity compared to alkane silanes and are thus used to protect perovskite films against moisture and water [181,182]. Wang et al. [181] demonstrated that the fluoro-silane trichloro(3,3,3-trifluoropropyl)silane ($C_3H_4Cl_3F_3Si$) will automatically undergoes a cross-linking process to form a robust layer to protect the underneath perovskite films from water attacking. The PVSCs with fluoro-silane layer without encapsulation showed negligible color change after soaking in water for 3 min, while the control device with 20 nm PCBM changed to yellow color after it was immersed in water for less than 5 s (Fig. 9a). Xiong et al. [182] used a fluoroalkyl silane triethoxy-1*H*,1*H*,2*H*,2*H*-tridecafluoro-*n*-octylsilane (C_{13}-FAS) to modify the perovskite films which were prepared in the full open space with a relative humidity of ~30%. The PVSCs reached a PCE of over 12.0 ± 0.4% and the PCE was maintained at ~12% for a duration of more than 500 h in air with a humidity of ~50%, while the efficiency of those without hydrophobic coating sharply decreased from ~12% to 1% in a duration of 250 h. The robust layer of organosilanes could also facilitate a post-treatment on the perovskite film. For example, Perumbalathodi et al. [183] demonstrated that (3-mercaptopropyl)trimethoxysilane (MPTMS) modified perovskite allows for the further deposition of CuSCN using diethyl sulfide.

On the other hand, SAMs formed by PACz derivatives [197], halogenated perfluorocarbons [188], thiols [117,196], perfluoroalkyl thiols [189] and carboxylic acids [190,191,193] have also been demonstrated to effectively reconstruct the perovskite surfaces to enhance device performance and stability simultaneously. For example, Mussakhanuly et al. [197] found that 2PACz at the interface induces favorable band bending at the interface, which prevents the funneling of carriers toward I-rich clusters. Instead, charge carriers funnel toward SAM, preventing the accumulation of polaron-induced strain on the lattice, and thus suppressing the phase segregation in Br/I mixed perovskite. Wolff et al. [188] introduced a SAM made of perfluorinated aliphatic carbon chains terminated with an iodine- or bromine-anchoring group (X-PFC_n) to modify perovskite films. The corresponding p-i-n cells exhibit PCEs above 21% with significantly improved stabilities against heat, light, and moisture. Zhang et al. [189] used 1*H*,1*H*,2*H*,2*H*-perfluorodecanethiol (PFDT) with a thiol headgroup and a perfluorocarbon tail-chain to form a closet-packed superhydrophobic SAM on the surface of perovskite and metal electrode. The thiol headgroup in SAMs can efficiently passivate the undercoordinated surface lead centers by forming Pb-S bond, leading to reduced defect densities on the perovskite film, while the rigid helical perfluorocarbon chains can tailor the surface properties of perovskite film and metal electrode, resulting in hydrophobic feature to physically impede moisture and oxygen permeation. These two advantages simultaneously immobilize lead ions and suppress lead leakage (Fig. 9b).

In addition to changing the hydrophobicity, the terminal groups of the SAM molecules also significantly affect other properties of the modified surfaces or grain boundaries, thereby subsequently influencing the performance and stability of PVSCs. This is particularly important in the cases of silane modification, as their terminal groups may point toward perovskites [184,185]. Xie et al. [184] introduced MPTMS in precursors to form a cross-linking siloxane network on the grain boundary which could modulate the crystallization, passivate the defects, and improve the thermal and moisture stability, outperforming the devices with modification of methoxysilane with -CH_3 (PTS) and -CN (CPTS) as terminal groups. The thiol group in MPTMS could also strongly interact with the undercoordinated Pb^{2+} at the perovskite surface, effectively minimizing interfacial charge recombination [183,199]. The presence of Cl atom in chloromethyltrimethoxysilane (CMS) and 3-chloropropyltrimethoxysilane (CPS) could efficiently passivate the iodine-vacancy trap states, thus prolonged photoluminescence lifetime could be achieved compared to the perovskite treated with methylsilane [185,200]. The polar Cl-terminated SAM molecules also modulate the energy-level alignment at perovskite/CTL interface for better charge extraction [185,190]. Therein, (3-Aminopropyl)trimethoxysilane (APTMS) with ammino as terminal groups was also demonstrated to efficiently reduce surface recombination velocity and thus enhance PCE in PVSCs by Shi et al. [186]. Recently, Soliman et al. [187] systematically investigated the influence of terminal groups of organosilanes on the device performance and stability by modifying the perovskites with a series of organosilanes with different chain lengths, fluorination, and different interactions toward perovskite. Terminal groups that show passivation ability toward perovskite are demonstrated to effectively reduce trap densities and thus improve the PCEs, while the fluorinated functional groups are beneficial for high stability. Finally, the PVSCs modified with 3,3,3-trifluoropropyltrimethoxysilane (FPTMS) achieved a high PCE of 23.0%. These devices also demonstrated the best operational stability, with the encapsulated device maintaining 85% of the initial PCE after 1725 h of operation in air.

The coverage of SAMs on ITO and metal oxide CTLs has been shown to be important for the device performance and stability, and the SAM packing properties such as orientation at ITO/perovskite interface have also been demonstrated to affect the charge extraction, but this has been less investigated. Liu et al. [195] found that, with the same terminal groups, 2-aminoethane-1-thiol hydrochloride (2AETCl), which has shorter alkyl chains compared to 2-aminopropane-1-thiol hydrochloride (2APTCl), exhibited a preference for parallel orientations, facilitating stronger interactions with surface defects through coordination and hydrogen bonding. Wang et al. [194] constructed a self-assembled cocrystal layer (SAM-CL) on perovskite by utilizing the intermolecular π-π interactions and hydrogen bonds between a 1-pyrenemethyl-amine hydrochloride (PRMA) monolayer on the perovskite surface and 2,3,5,6-tetrafluoro-7,7′,8,8′-tetracyanoquinodimethane (F4TCNQ) doped in spiro-OMeTAD (Fig. 9c). The SAM-CL optimizes interfacial energy level alignment to eliminate the interfacial charge accumulation. The large pyrene rings and fluorine atoms in SAM-CL also effectively hinders ion migration and moisture invasion, significantly improving the stability of PVSCs. The passivating ligands usually bind to a single active binding site on perovskite, and the dense packing of electrically resistive molecules perpendicular to the surface may limit the FF in PVSCs. To address this, Chen et al. [198] recently used 4-chlorobenzenesulfonate (4Cl-BZS) as passivating ligand, which binds two neighboring Pb^{2+} defect sites in a planar ligand orientation on the perovskite. The corresponding PVSCs show a certified PCE of 26.15% with a T_{95} of 1200 h under continuous 1 sun MPP tracking at 65 °C.

5. Conclusions and outlook

We have systematically summarized the development and progress on applications of SAMs for interfacial engineering in PVSCs at different interfaces.

Strategies such as co-SAM, processing solvent optimization, surface pretreatment and molecular design could improve the density and coverage of monolayers on ITO. Strong acid-based molecules such as the widely used PACz derivatives are favorable for dense monolayers, but unfavorable for the long-term stability of ITO. The inherent difficulty in achieving stable and uniform SAM coverage on ITO remains a challenge. The co-SAM strategy by mixing molecules with different anchoring

groups may be suitable for achieving the balance of dense and stable SAMs for long-term stability of the ITO interface in PVSCs. Designing SAM molecules with multiple anchoring groups may also enhance binding affinity to ITO, resulting in more stable and uniform coverage. For practical implementation, an integrated approach combining molecular design, surface pretreatment, solvent optimization, and the co-SAM strategy is recommended.

The orientation of the SAM molecules on electrode and perovskite surfaces shows significant impact on the charge extraction, transport and recombination. However, research on this aspect remains limited. Additionally, SAM orientation at the CTLs interface may also influence the WF tuning, interfacial charge transfer, and the adhesion between CTLs and the overlying perovskite layers. Studies focusing on SAM molecular orientation at these interfaces may further improve the device performance and stability by improving charge extraction, reducing energy losses and minimizing recombination.

Although lots of SAM molecules have been synthesized to achieve interfaces with desired properties, the traditional approach to designing SAMs involves trial-and-error experiments, which can be slow, costly, and inefficient. Artificial Intelligence (AI)-assisted SAM design offers tremendous potential to optimize the interface properties in PVSCs. However, challenges remain, including the need for high-quality data, accurate modeling of complex SAM-interface interactions, and integration with experimental validation. Moving forward, a hybrid AI-experimental approach, combined with advanced simulations and a more comprehensive dataset, will be critical to accelerating the development of high-performance, stable, and commercially viable PVSCs.

Spin-coating is the most used processing method for SAMs in current PVSC research. However, upscaling deposition methods, such as roll-to-roll or spray coating, should be investigated and developed, as they are essential for large-area PVSC fabrication. The challenges related to uniformity, repeatability, and cost-effectiveness must be addressed. Additionally, the principles for achieving SAMs with the desired properties through spin-coating may need to be adjusted.

CRediT authorship contribution statement

Weifei Fu: Writing – review & editing, Supervision, Project administration, Funding acquisition. **Ahmed I.A. Soliman:** Writing – original draft, Investigation. **Yiran Zheng:** Investigation. **Yu Zhou:** Investigation. **Yiqing Zhang:** Investigation. **Shiqi Shan:** Investigation. **Hongzheng Chen:** Writing – review & editing, Supervision, Project administration, Funding acquisition.

Declaration of competing interest

The authors declare that they have no known competing financial interests or personal relationships that could have appeared to influence the work reported in this paper.

Acknowledgements

This work was supported by the National Natural Science Foundation of China (Grant Nos. 52472256 and 52103324), the Natural Science Foundation of Zhejiang Province (No. LD24E030002), and the Fundamental Research Funds for the Central Universities (226-2024-00005, 226-2024-00056). AIAS acknowledges the International Postdoctoral Exchange Fellowship Program (Talent-Introduction Program) for financial support.

Appendix A. Supplementary data

Supplementary data to this article can be found online at https://doi.org/10.1016/j.revmat.2025.100017.

References

[1] J.Y. Kim, J.-W. Lee, H.S. Jung, H. Shin, N.-G. Park, High-efficiency perovskite solar cells, Chem. Rev. 120 (2020) 7867–7918, https://doi.org/10.1021/acs.chemrev.0c00107.
[2] National Renewable Energy Laboratory (NREL), Best research-cell efficiency chart, Available online: https://www.nrel.gov/pv/cell-efficiency.html. (Accessed 7 April 2025).
[3] L. Duan, D. Walter, N. Chang, J. Bullock, D. Kang, S.P. Phang, K. Weber, T. White, D. Macdonald, K. Catchpole, H. Shen, Stability challenges for the commercialization of perovskite–silicon tandem solar cells, Nat. Rev. Mater. 8 (2023) 261–281, https://doi.org/10.1038/s41578-022-00521-1.
[4] C.-C. Chueh, C.-Z. Li, A.K.Y. Jen, Recent progress and perspective in solution-processed Interfacial materials for efficient and stable polymer and organometal perovskite solar cells, Energy Environ. Sci. 8 (2015) 1160–1189, https://doi.org/10.1039/C4EE03824J.
[5] Y. Li, H. Xie, E.L. Lim, A. Hagfeldt, D. Bi, Recent progress of critical interface engineering for highly efficient and stable perovskite solar cells, Adv. Energy Mater. 12 (2022) 2102730, https://doi.org/10.1002/aenm.202102730.
[6] Y.-C. Chin, M. Daboczi, C. Henderson, J. Luke, J.-S. Kim, Suppressing PEDOT:PSS doping-induced interfacial recombination loss in perovskite solar cells, ACS Energy Lett. 7 (2022) 560–568, https://doi.org/10.1021/acsenergylett.1c02577.
[7] Y. Wang, L. Duan, M. Zhang, Z. Hameiri, X. Liu, Y. Bai, X. Hao, PTAA as efficient hole transport materials in perovskite solar cells: a review, Sol. RRL 6 (2022) 2200234, https://doi.org/10.1002/solr.202200234.
[8] P. Schulz, J.O. Tiepelt, J.A. Christians, I. Levine, E. Edri, E.M. Sanehira, G. Hodes, D. Cahen, A. Kahn, High-work-function molybdenum oxide hole extraction contacts in hybrid organic–inorganic perovskite solar cells, ACS Appl. Mater. Interfaces 8 (2016) 31491–31499, https://doi.org/10.1021/acsami.6b10898.
[9] W. Chen, Y. Wu, Y. Yue, J. Liu, W. Zhang, X. Yang, H. Chen, E. Bi, I. Ashraful, M. Grätzel, L. Han, Efficient and stable large-area perovskite solar cells with inorganic charge extraction layers, Science 350 (2015) 944–948, https://doi.org/10.1126/science.aad1015.
[10] X. Yin, Y. Guo, H. Xie, W. Que, L.B. Kong, Nickel oxide as efficient hole transport materials for perovskite solar cells, Sol. RRL 3 (2019) 1900001, https://doi.org/10.1002/solr.201900001.
[11] W. Hu, S. Yang, S. Yang, Surface modification of TiO_2 for perovskite solar cells, Trends Chem. 2 (2020) 148–162, https://doi.org/10.1016/j.trechm.2019.11.002.
[12] P. Zhang, J. Wu, T. Zhang, Y. Wang, D. Liu, H. Chen, L. Ji, C. Liu, W. Ahmad, Z.D. Chen, S. Li, Perovskite solar cells with ZnO electron-transporting materials, Adv. Mater. 30 (2018) 1703737, https://doi.org/10.1002/adma.201703737.
[13] Q. Jiang, X. Zhang, J. You, SnO_2: a wonderful electron transport layer for perovskite solar cells, Small 14 (2018) 1801154, https://doi.org/10.1002/smll.201801154.
[14] H. Choi, C.-K. Mai, H.-B. Kim, J. Jeong, S. Song, G.C. Bazan, J.Y. Kim, A.J. Heeger, Conjugated polyelectrolyte hole transport layer for inverted-type perovskite solar cells, Nat. Commun. 6 (2015) 7348, https://doi.org/10.1038/ncomms8348.
[15] J. Hu, W. Fu, X. Yang, H. Chen, Self-assembled monolayers for interface engineering in polymer solar cells, J. Polym. Sci. 60 (2022) 2175–2190, https://doi.org/10.1002/pol.20210938.
[16] S.Y. Kim, S.J. Cho, S.E. Byeon, X. He, H.J. Yoon, Self-assembled monolayers as interface engineering nanomaterials in perovskite solar cells, Adv. Energy Mater. 10 (2020) 2002606, https://doi.org/10.1002/aenm.202002606.
[17] J. Hu, C. He, X. Zheng, Y. Li, X. Yang, W. Wang, J. Zhang, Q. Chen, F. Huang, W. Fu, H. Chen, Tailoring self-assembled monolayers for high-performance polymer solar cells with improved stability, Sol. RRL 7 (2023) 2201106, https://doi.org/10.1002/solr.202201106.
[18] S. Guan, Y. Li, C. Xu, N. Yin, C. Xu, C. Wang, M. Wang, Y. Xu, Q. Chen, D. Wang, L. Zuo, H. Chen, Self-assembled interlayer enables high-performance organic photovoltaics with power conversion efficiency exceeding 20%, Adv. Mater. 36 (2024) 2400342 https://doi.org/10.1002/adma.202400342.
[19] M. Li, M. Liu, F. Qi, F.R. Lin, A.K.Y. Jen, Self-assembled monolayers for interfacial engineering in solution-processed thin-film electronic devices: design, fabrication, and applications, Chem. Rev. 124 (2024) 2138–2204, https://doi.org/10.1021/acs.chemrev.3c00396.
[20] S. Casalini, C.A. Bortolotti, F. Leonardi, F. Biscarini, Self-assembled monolayers in organic electronics, Chem. Soc. Rev. 46 (2017) 40–71, https://doi.org/10.1039/c6cs00509h.
[21] Y. Hou, S. Scheiner, X. Tang, N. Gasparini, M. Richter, N. Li, P. Schweizer, S. Chen, H. Chen, C.O.R. Quiroz, X. Du, G.J. Matt, A. Osvet, E. Spiecker, R.H. Fink, A. Hirsch, M. Halik, C.J. Brabec, Suppression of hysteresis effects in organohalide perovskite solar cells, Adv. Mater. Interfaces 4 (2017) 1700007, https://doi.org/10.1002/admi.201700007.
[22] Y. Hou, X. Du, S. Scheiner, D.P. McMeekin, Z. Wang, N. Li, M.S. Killian, H. Chen, M. Richter, I. Levchuk, N. Schrenker, E. Spiecker, T. Stubhan, N.A. Luechinger, A. Hirsch, P. Schmuki, H.-P. Steinrück, R.H. Fink, M. Halik, H.J. Snaith, C.J. Brabec, A generic interface to reduce the efficiency-stability-cost gap of perovskite solar cells, Science 358 (2017) 1192–1197, https://doi.org/10.1126/science.aao5561.
[23] P. Topolovsek, F. Lamberti, T. Gatti, A. Cito, J.M. Ball, E. Menna, C. Gadermaier, A. Petrozza, Functionalization of transparent conductive oxide electrode for TiO_2-free perovskite solar cells, J. Mater. Chem. A 5 (2017) 11882–11893, https://doi.org/10.1039/C7TA02405C.
[24] H. Cheng, Y. Li, M. Zhang, K. Zhao, Z.-S. Wang, Self-assembled ionic liquid for highly efficient electron transport layer-free perovskite solar cells, ChemSusChem 13 (2020) 2779–2785, https://doi.org/10.1002/cssc.202000342.

[25] S.O. Fürer, K.J. Rietwyk, F. Pulvirenti, D.P. McMeekin, M.A. Surmiak, S.R. Raga, W. Mao, X. Lin, Y. Hora, J. Wang, Y. Shi, S. Barlow, D.S. Ginger, S.R. Marder, U. Bach, Naphthalene-imide self-assembled monolayers as a surface modification of ITO for improved thermal stability of perovskite solar cells, ACS Appl. Energy Mater. 6 (2023) 667–677, https://doi.org/10.1021/acsaem.2c02735.
[26] D.S. Utomo, L.M. Svirskaite, A. Prasetio, V. Malinauskiene, P. Dally, E. Aydin, A. Musiienko, V. Getautis, T. Malinauskas, R. Azmi, S. De Wolf, Nonfullerene self-assembled monolayers as electron-selective contacts for n-i-p perovskite solar cells, ACS Energy Lett. 9 (2024) 1682–1692, https://doi.org/10.1021/acsenergylett.4c00306.
[27] A. Magomedov, A. Al-Ashouri, E. Kasparavičius, S. Strazdaite, G. Niaura, M. Jošt, T. Malinauskas, S. Albrecht, V. Getautis, Self-assembled hole transporting monolayer for highly efficient perovskite solar cells, Adv. Energy Mater. 8 (2018) 1801892, https://doi.org/10.1002/aenm.201801892.
[28] A. Al-Ashouri, A. Magomedov, M. Roß, M. Jošt, M. Talaikis, G. Chistiakova, T. Bertram, J.A. Márquez, E. Köhnen, E. Kasparavičius, S. Levcenco, L. Gil-Escrig, C.J. Hages, R. Schlatmann, B. Rech, T. Malinauskas, T. Unold, C.A. Kaufmann, L. Korte, G. Niaura, V. Getautis, S. Albrecht, Conformal monolayer contacts with lossless interfaces for perovskite single junction and monolithic tandem solar cells, Energy Environ. Sci. 12 (2019) 3356–3369, https://doi.org/10.1039/C9EE02268F.
[29] A. Al-Ashouri, E. Köhnen, B. Li, A. Magomedov, H. Hempel, P. Caprioglio, J.A. Márquez, A.B. Morales Vilches, E. Kasparavicius, J.A. Smith, N. Phung, D. Menzel, M. Grischek, L. Kegelmann, D. Skroblin, C. Gollwitzer, T. Malinauskas, M. Jošt, G. Matič, B. Rech, R. Schlatmann, M. Topič, L. Korte, A. Abate, B. Stannowski, D. Neher, M. Stolterfoht, T. Unold, V. Getautis, S. Albrecht, Monolithic perovskite/silicon tandem solar cell with >29% efficiency by enhanced hole extraction, Science 370 (2020) 1300–1309, https://doi.org/10.1126/science.abd4016.
[30] I. Levine, A. Al-Ashouri, A. Musiienko, H. Hempel, A. Magomedov, A. Drevilkauskaite, V. Getautis, D. Menzel, K. Hinrichs, T. Unold, S. Albrecht, T. Dittrich, Charge transfer rates and electron trapping at buried interfaces of perovskite solar cells, Joule 5 (2021) 2915–2933, https://doi.org/10.1016/j.joule.2021.07.016.
[31] M. Pitaro, J.E.S. Alonso, L. Di Mario, D.G. Romero, K. Tran, J. Kardula, T. Zaharia, M.B. Johansson, E.M.J. Johansson, R.C. Chiechi, M.A. Loi, Tuning the surface energy of hole transport layers based on carbazole self-assembled monolayers for highly efficient Sn/Pb perovskite solar cells, Adv. Funct. Mater. 34 (2024) 2306571, https://doi.org/10.1002/adfm.202306571.
[32] H. Zhou, W. Wang, Y. Duan, R. Sun, Y. Li, Z. Xie, D. Xu, M. Wu, Y. Wang, H. Li, Q. Fan, Y. Peng, Y. Yao, C. Liao, Q. Peng, S. Liu, Z. Liu, Glycol monomethyl ether-substituted carbazolyl hole-transporting material for stable inverted perovskite solar cells with efficiency of 25.52%, Angew. Chem. Int. Ed. 63 (2024) e202403068 https://doi.org/10.1002/anie.202403068.
[33] A. Sun, C. Tian, R. Zhuang, C. Chen, Y. Zheng, X. Wu, C. Tang, Y. Liu, Z. Li, B. Ouyang, J. Du, Z. Li, J. Cai, J. Chen, X. Wu, Y. Hua, C.C. Chen, High open-circuit voltage (1.197 V) in large-area (1 cm^2) inverted perovskite solar cell via interface planarization and highly polar self-assembled monolayer, Adv. Energy Mater. 14 (2024) 2303941, https://doi.org/10.1002/aenm.202303941.
[34] Z. Dai, S. You, D. Chakraborty, S. Li, Y. Zhang, A. Ranka, S. Barlow, J.J. Berry, S.R. Marder, P. Guo, Y. Qi, K. Zhu, N.P. Padture, Connecting interfacial mechanical adhesion, efficiency, and operational stability in high performance inverted perovskite solar cells, ACS Energy Lett. 9 (2024) 1880–1887, https://doi.org/10.1021/acsenergylett.4c00510.
[35] W. Jiang, F. Li, M. Li, F. Qi, F.R. Lin, A.K.-Y. Jen, π-Expanded carbazoles as hole-selective self-assembled monolayers for high-performance perovskite solar cells, Angew. Chem. Int. Ed. 61 (2022) e202213560, https://doi.org/10.1002/anie.202213560.
[36] W. Wang, K. Wei, L. Yang, J. Deng, J. Zhang, W. Tang, Dynamic self-assembly of small molecules enables the spontaneous fabrication of hole conductors at perovskite/electrode interfaces for over 22% stable inverted perovskite solar cells, Mater. Horiz. 10 (2023) 2609–2617, https://doi.org/10.1039/D3MH00219E.
[37] R. He, W. Wang, Z. Yi, F. Lang, C. Chen, J. Luo, J. Zhu, J. Thiesbrummel, S. Shah, K. Wei, Y. Luo, C. Wang, H. Lai, H. Huang, J. Zhou, B. Zou, X. Yin, S. Ren, X. Hao, L. Wu, J. Zhang, J. Zhang, M. Stolterfoht, F. Fu, W. Tang, D. Zhao, Improving interface quality for 1-cm^2 all-perovskite tandem solar cells, Nature 618 (2023) 80–86, https://doi.org/10.1038/s41586-023-05992-y.
[38] W. Wang, X. Liu, J. Wang, C. Chen, J. Yu, D. Zhao, W. Tang, Versatile self-assembled molecule enables high-efficiency wide-bandgap perovskite solar cells and organic solar cells, Adv. Energy Mater. 13 (2023) 2300694, https://doi.org/10.1002/aenm.202300694.
[39] Z. Yi, W. Wang, R. He, J. Zhu, W. Jiao, Y. Luo, Y. Xu, Y. Wang, Z. Zeng, K. Wei, J. Zhang, S.-W. Tsang, C. Chen, W. Tang, D. Zhao, Achieving a high open-circuit voltage of 1.339 V in 1.77 eV wide-bandgap perovskite solar cells via self-assembled monolayers, Energy Environ. Sci. 17 (2024) 202–209, https://doi.org/10.1039/D3EE02839A.
[40] W. Jiang, M. Liu, Y. Li, F.R. Lin, A.K.Y. Jen, Rational molecular design of multifunctional self-assembled monolayers for efficient hole selection and buried interface passivation in inverted perovskite solar cells, Chem. Sci. 15 (2024) 2778–2785, https://doi.org/10.1039/d3sc05485c.
[41] C. Li, Z. Zhang, H. Zhang, W. Yan, Y. Li, L. Liang, W. Yu, X. Yu, Y. Wang, Y. Yang, M.K. Nazeeruddin, P. Gao, Fully aromatic self-assembled hole-selective layer toward efficient inverted wide-bandgap perovskite solar cells with ultraviolet resistance, Angew. Chem. Int. Ed. 63 (2024) e202315281, https://doi.org/10.1002/anie.202315281.
[42] G. Qu, S. Cai, Y. Qiao, D. Wang, S. Gong, D. Khan, Y. Wang, K. Jiang, Q. Chen, L. Zhang, Y.-G. Wang, X. Chen, A.K.Y. Jen, Z.-X. Xu, Conjugated linker-boosted self-assembled monolayer molecule for inverted perovskite solar cells, Joule 8 (2024) 2123–2134, https://doi.org/10.1016/j.joule.2024.05.005.
[43] Z. Ren, Z. Cui, X. Shi, L. Wang, Y. Dou, F. Wang, H. Lin, H. Yan, S. Chen, Poly(carbazole phosphonic acid) as a versatile hole-transporting material for p-i-n perovskite solar cells and modules, Joule 7 (2023) 2894–2904, https://doi.org/10.1016/j.joule.2023.10.014.
[44] W. Jiang, Y. Hu, F. Li, F.R. Lin, A.K.Y. Jen, Hole-selective contact with molecularly tailorable reactivity for passivating high-performing inverted perovskite solar cells, CCS Chem. 6 (2024) 1654–1661, https://doi.org/10.31635/ccschem.024.202303710.
[45] Y. Zheng, C. Tian, X. Wu, A. Sun, R. Zhuang, C. Tang, Y. Liu, Z. Li, B. Ouyang, J. Du, Z. Li, X. Wu, J. Chen, J. Cai, C.C. Chen, Dual-interface modification for inverted methylammonium-free perovskite solar cells of 25.35% efficiency with balanced crystallization, Adv. Energy Mater. 14 (2024) 2304486, https://doi.org/10.1002/aenm.202304486.
[46] X. Deng, F. Qi, F. Li, S. Wu, F.R. Lin, Z. Zhang, Z. Guan, Z. Yang, C.-S. Lee, A.K.-Y. Jen, Co-Assembled monolayers as hole-selective contact for high-performance inverted perovskite solar cells with optimized recombination loss and long-term stability, Angew. Chem. Int. Ed. 61 (2022) e202203088, https://doi.org/10.1002/anie.202203088.
[47] E. Li, C. Liu, H. Lin, X. Xu, S. Liu, S. Zhang, M. Yu, X.-M. Cao, Y. Wu, W.-H. Zhu, Bonding strength regulates anchoring-based self-assembly monolayers for efficient and stable perovskite solar cells, Adv. Funct. Mater. 31 (2021) 2103847, https://doi.org/10.1002/adfm.202103847.
[48] A. Ullah, K.H. Park, H.D. Nguyen, Y. Siddique, S.F.A. Shah, H. Tran, S. Park, S.I. Lee, K.-K. Lee, C.-H. Han, K. Kim, S. Ahn, I. Jeong, Y.S. Park, S. Hong, Novel phenothiazine-based self-assembled monolayer as a hole selective contact for highly efficient and stable p-i-n perovskite solar cells, Adv. Energy Mater. 12 (2022) 2103175, https://doi.org/10.1002/aenm.202103175.
[49] A. Ullah, K.H. Park, Y. Lee, S. Park, A.B. Faheem, H.D. Nguyen, Y. Siddique, K.-K. Lee, Y. Jo, C.-H. Han, S. Ahn, I. Jeong, S. Cho, B. Kim, Y.S. Park, S. Hong, Versatile hole selective molecules containing a series of heteroatoms as self-assembled monolayers for efficient p-i-n perovskite and organic solar cells, Adv. Funct. Mater. 32 (2022) 2208793, https://doi.org/10.1002/adfm.202208793.
[50] M. Li, Z. Li, M. Liu, H. Fu, F. Qi, F.R. Lin, A. Walsh, A.K.Y. Jen, A hole-selective self-assembled monolayer for both efficient perovskite and organic solar cells, Langmuir 40 (2024) 4772–4778, https://doi.org/10.1021/acs.langmuir.3c03610.
[51] S. Zhang, F. Ye, X. Wang, R. Chen, H. Zhang, L. Zhan, X. Jiang, Y. Li, X. Ji, S. Liu, M. Yu, F. Yu, Y. Zhang, R. Wu, Z. Liu, Z. Ning, D. Neher, L. Han, Y. Lin, H. Tian, W. Chen, M. Stolterfoht, L. Zhang, W.-H. Zhu, Y. Wu, Minimizing buried interfacial defects for efficient inverted perovskite solar cells, Science 380 (2023) 404–409, https://doi.org/10.1126/science.adg3755.
[52] G. Kapil, T. Bessho, Y. Sanehira, S.R. Sahamir, M. Chen, A.K. Baranwal, D. Liu, Y. Sono, D. Hirotani, D. Nomura, K. Nishimura, M.A. Kamarudin, Q. Shen, H. Segawa, S. Hayase, Tin–lead perovskite solar cells fabricated on hole selective monolayers, ACS Energy Lett. 7 (2022) 966–974, https://doi.org/10.1021/acsenergylett.1c02718.
[53] M. Liu, M.L. Li, Y.X. Li, Y.D. An, Z.F. Yao, B.B. Fan, F. Qi, K.K. Liu, H.L. Yip, F.R. Lin, A.K.Y. Jen, Defect-passivating and stable benzothiophene-based self-assembled monolayer for high-performance inverted perovskite solar cells, Adv. Energy Mater. 14 (2024) 2303742, https://doi.org/10.1002/aenm.202303742.
[54] A. Al-Ashouri, M. Marčinskas, E. Kasparavičius, T. Malinauskas, A. Palmstrom, V. Getautis, S. Albrecht, M.D. McGehee, A. Magomedov, Wettability improvement of a carbazole-based hole-selective monolayer for reproducible perovskite solar cells, ACS Energy Lett. 8 (2023) 898–900, https://doi.org/10.1021/acsenergylett.2c02629.
[55] N. Singh, A. Mohapatra, C.-W. Chu, Y.-T. Tao, Modulation of work function of ITO by self-assembled monolayer and its effect on device characteristics of inverted perovskite solar cells, Org. Electron. 98 (2021) 106297, https://doi.org/10.1016/j.orgel.2021.106297.
[56] M.A. Truong, T. Funasaki, L. Ueberricke, W. Nojo, R. Murdey, T. Yamada, S. Hu, A. Akatsuka, N. Sekiguchi, S. Hira, L. Xie, T. Nakamura, N. Shioya, D. Kan, Y. Tsuji, S. Iikubo, H. Yoshida, Y. Shimakawa, T. Hasegawa, Y. Kanemitsu, T. Suzuki, A. Wakamiya, Tripodal triazatruxene derivative as a face-on oriented hole-collecting monolayer for efficient and stable inverted perovskite solar cells, J. Am. Chem. Soc. 145 (2023) 7528–7539, https://doi.org/10.1021/jacs.3c00805.
[57] M.A. Truong, L. Ueberricke, T. Funasaki, Y. Adachi, S. Hira, S. Hu, T. Yamada, N. Sekiguchi, T. Nakamura, R. Murdey, S. Iikubo, Y. Kanemitsu, A. Wakamiya, Tetrapodal hole-collecting monolayer materials based on saddle-like cyclooctatetraene core for inverted perovskite solar cells, Angew. Chem. Int. Ed. 63 (2024) e202412939, https://doi.org/10.1002/anie.202412939.
[58] S. Zhang, R. Wu, C. Mu, Y. Wang, L. Han, Y. Wu, W.-H. Zhu, Conjugated self-assembled monolayer as stable hole-selective contact for inverted perovskite solar cells, ACS Mater. Lett. 4 (2022) 1976–1983, https://doi.org/10.1021/acsmaterialslett.2c00799.
[59] Q. Liao, Y. Wang, Z. Zhang, K. Yang, Y. Shi, K. Feng, B. Li, J. Huang, P. Gao, X. Guo, Self-assembled donor-acceptor hole contacts for inverted perovskite solar cells with an efficiency approaching 22%: the impact of anchoring groups, J. Energy Chem. 68 (2022) 87–95, https://doi.org/10.1016/j.jechem.2021.11.001.
[60] X. Sun, H. Fan, X. Xu, G. Li, X. Gu, D. Luo, C. Shan, Q. Yang, S. Dong, C. Miao, Z. Xie, G. Lu, D.H. Wang, P.P. Sun, A.K.K. Kyaw, A fluorination strategy and low-acidity anchoring group in self-assembled molecules for efficient and stable

inverted perovskite solar cells, Chem. Eur J. 30 (2024) e202400629, https://doi.org/10.1002/chem.202400629.
[61] E. Arkan, E. Yalcin, M. Unal, M.Z.Y. Arkan, M. Can, C. Tozlu, S. Demic, Effect of functional groups of self assembled monolayer molecules on the performance of inverted perovskite solar cell, Mater. Chem. Phys. 254 (2020) 123435, https://doi.org/10.1016/j.matchemphys.2020.123435.
[62] E. Arkan, M. Unal, E. Yalcin, M.Z. Yigit Arkan, S. Yurtdas, M. Can, C. Tozlu, S. Demic, Influence of end groups variation of self assembled monolayers on performance of planar perovskite solar cells by interface regulation, Mater. Sci. Semicond. Process. 123 (2021) 105514, https://doi.org/10.1016/j.mssp.2020.105514.
[63] E. Arkan, M.Z. Yigit Arkan, M. Unal, E. Yalcin, H. Aydin, C. Celebi, M. Can, C. Tozlu, S. Demic, Performance enhancement of inverted perovskite solar cells through interface engineering by TPD based bidentate self-assembled monolayers, Opt. Mater. 105 (2020) 109910, https://doi.org/10.1016/j.optmat.2020.109910.
[64] J. Zhang, Y. Sun, H. Yu, Reducing energy loss via adjusting the anode work function and perovskite layer morphology for the efficient and stable hole transporting layer-free perovskite solar cells, Chem. Eng. J. 431 (2022) 133948, https://doi.org/10.1016/j.cej.2021.133948.
[65] S.M. Park, M. Wei, N. Lempesis, W. Yu, T. Hossain, L. Agosta, V. Carnevali, H.R. Atapattu, P. Serles, F.T. Eickemeyer, H. Shin, M. Vafaie, D. Choi, K. Darabi, E.D. Jung, Y. Yang, D.B. Kim, S.M. Zakeeruddin, B. Chen, A. Amassian, T. Filleter, M.G. Kanatzidis, K.R. Graham, L. Xiao, U. Rothlisberger, M. Grätzel, E.H. Sargent, Low-loss contacts on textured substrates for inverted perovskite solar cells, Nature 624 (2023) 289–294, https://doi.org/10.1038/s41586-023-06745-7.
[66] H. Tang, Z. Shen, Y. Shen, G. Yan, Y. Wang, Q. Han, L. Han, Reinforcing self-assembly of hole transport molecules for stable inverted perovskite solar cells, Science 383 (2024) 1236–1240, https://doi.org/10.1126/science.adj9602.
[67] E. Yalcin, M. Can, C. Rodriguez-Seco, E. Aktas, R. Pudi, W. Cambarau, S. Demic, E. Palomares, Semiconductor self-assembled monolayers as selective contacts for efficient PiN perovskite solar cells, Energy Environ. Sci. 12 (2019) 230–237, https://doi.org/10.1039/C8EE01831F.
[68] E. Aktas, N. Phung, H. Köbler, D.A. González, M. Méndez, I. Kafedjiska, S.-H. Turren-Cruz, R. Wenisch, I. Lauermann, A. Abate, E. Palomares, Understanding the perovskite/self-assembled selective contact interface for ultra-stable and highly efficient *p–i–n* perovskite solar cells, Energy Environ. Sci. 14 (2021) 3976–3985, https://doi.org/10.1039/D0EE03807E.
[69] D.A. González, C.E. Puerto Galvis, W. Li, M. Méndez, E. Aktas, M.-F. Eugenia, E. Palomares, Influence of the carbazole moiety in self-assembling molecules as selective contacts in perovskite solar cells: interfacial charge transfer kinetics and solar-to-energy efficiency effects, Nanoscale Adv. 5 (2023) 6542–6547, https://doi.org/10.1039/D3NA00811H.
[70] A.V. Kesavan, V. Adiga, G.K. Chandrasekar, K.M. Panidhara, P.C. Ramamurthy, Nanoscale small molecule self-assembled ITO for photon harvesting in polymer and perovskite solar cells, Sol. Energy 240 (2022) 201–210, https://doi.org/10.1016/j.solener.2022.05.002.
[71] A. Abid, P. Rajamanickam, E. Wei-Guang Diau, Design of a simple bifunctional system as a self-assembled monolayer (SAM) for inverted tin-based perovskite solar cells, Chem. Eng. J. 477 (2023) 146755, https://doi.org/10.1016/j.cej.2023.146755.
[72] S.N. Afraj, C.-H. Kuan, J.-S. Lin, J.-S. Ni, A. Velusamy, M.-C. Chen, E.W.-G. Diau, Quinoxaline-based X-shaped sensitizers as self-assembled monolayer for tin perovskite solar cells, Adv. Funct. Mater. 33 (2023) 2213939, https://doi.org/10.1002/adfm.202213939.
[73] W. Li, M. Cariello, M. Méndez, G. Cooke, E. Palomares, Self-assembled molecules for hole-selective electrodes in highly stable and efficient inverted perovskite solar cells with ultralow energy loss, ACS Appl. Energy Mater. 6 (2023) 1239–1247, https://doi.org/10.1021/acsaem.2c02880.
[74] E. Aktas, J. Jiménez-López, K. Azizi, T. Torres, E. Palomares, Self-assembled Zn phthalocyanine as a robust p-type selective contact in perovskite solar cells, Nanoscale Horiz 5 (2020) 1415–1419, https://doi.org/10.1039/D0NH00443J.
[75] C.-M. Hung, C.-L. Mai, C.-C. Wu, B.-H. Chen, C.-H. Lu, C.-C. Chu, M.-C. Wang, S.-D. Yang, H.-C. Chen, C.-Y. Yeh, P.-T. Chou, Self-assembled monolayers of Bi-functionalized porphyrins: a novel class of hole-layer-coordinating perovskites and indium tin oxide in inverted solar cells, Angew. Chem. Int. Ed. 62 (2023) e202309831, https://doi.org/10.1002/anie.202309831.
[76] E. Aktas, R. Pudi, N. Phung, R. Wenisch, L. Gregori, D. Meggiolaro, M.A. Flatken, F. De Angelis, I. Lauermann, A. Abate, E. Palomares, Role of terminal group position in triphenylamine-based self-assembled hole-selective molecules in perovskite solar cells, ACS Appl. Mater. Interfaces 14 (2022) 17461–17469, https://doi.org/10.1021/acsami.2c01981.
[77] E. Yalcin, E. Aktas, M. Mendéz, E. Arkan, J.G. Sánchez, E. Martínez-Ferrero, F. Silvestri, E. Barrena, M. Can, S. Demic, E. Palomares, Monodentate versus bidentate anchoring groups in self-assembling molecules (SAMs) for robust *p–i–n* perovskite solar cells, ACS Appl. Mater. Interfaces 15 (2023) 57153–57164, https://doi.org/10.1021/acsami.3c13727.
[78] H. Cheng, Z.-S. Huang, Self-assembled organic molecules with a fused aromatic ring as hole-transport layers for inverted perovskite solar cells: the effect of linkers on performance, New J. Chem. 48 (2024) 6833–6841, https://doi.org/10.1039/D4NJ00154K.
[79] Z. Zhang, R. Zhu, Y. Tang, Z. Su, S. Hu, X. Zhang, J. Zhang, J. Zhao, Y. Xue, X. Gao, G. Li, J. Pascual, A. Abate, M. Li, Anchoring charge selective self-assembled monolayers for tin–lead perovskite solar cells, Adv. Mater. 36 (2024) 2312264, https://doi.org/10.1002/adma.202312264.
[80] D. Akın Kara, K. Kara, G. Oylumluoglu, M.Z. Yigit, M. Can, J.J. Kim, E.K. Burnett, D.L. Gonzalez Arellano, S. Buyukcelebi, F. Ozel, O. Usluer, A.L. Briseno, M. Kus, Enhanced device efficiency and long-term stability via boronic acid-based self-assembled monolayer modification of indium tin oxide in a planar perovskite solar cell, ACS Appl. Mater. Interfaces 10 (2018) 30000–30007, https://doi.org/10.1021/acsami.8b10445.
[81] H. Guo, C. Liu, H. Hu, S. Zhang, X. Ji, X.-M. Cao, Z. Ning, W.-H. Zhu, H. Tian, Y. Wu, Neglected acidity pitfall: boric acid-anchoring hole-selective contact for perovskite solar cells, Natl. Sci. Rev. 10 (2023) nwad057, https://doi.org/10.1093/nsr/nwad057.
[82] M. Liu, L. Bi, W. Jiang, Z. Zeng, S.-W. Tsang, F.R. Lin, A.K.-Y. Jen, Compact hole-selective self-assembled monolayers enabled by disassembling micelles in solution for efficient perovskite solar cells, Adv. Mater. 35 (2023) 2304415, https://doi.org/10.1002/adma.202304415.
[83] A. Kulkarni, R. Sarkar, S. Akel, M. Häser, B. Klingebiel, M. Wuttig, S. Wiegand, S. Chakraborty, M. Saliba, T. Kirchartz, A universal strategy of perovskite ink-substrate interaction to overcome the poor wettability of a self-assembled monolayer for reproducible perovskite solar cells, Adv. Funct. Mater. 33 (2023) 2305812, https://doi.org/10.1002/adfm.202305812.
[84] P. Tockhorn, J. Sutter, A. Cruz, P. Wagner, K. Jäger, D. Yoo, F. Lang, M. Grischek, B. Li, J. Li, O. Shargaieva, E. Unger, A. Al-Ashouri, E. Köhnen, M. Stolterfoht, D. Neher, R. Schlatmann, B. Rech, B. Stannowski, S. Albrecht, C. Becker, Nano-optical designs for high-efficiency monolithic perovskite–silicon tandem solar cells, Nat. Nanotech. 17 (2022) 1214–1221, https://doi.org/10.1038/s41565-022-01228-8.
[85] M. Taddei, J.A. Smith, B.M. Gallant, S. Zhou, R.J.E. Westbrook, Y. Shi, J. Wang, J.N. Drysdale, D.P. McCarthy, S. Barlow, S.R. Marder, H.J. Snaith, D.S. Ginger, Ethylenediamine addition improves performance and suppresses phase instabilities in mixed-halide perovskites, ACS Energy Lett. 7 (2022) 4265–4273, https://doi.org/10.1021/acsenergylett.2c01998.
[86] W.H.K. Perera, M.G. Masteghin, H. Shim, J.D. Davies, J.L. Ryan, S.J. Hinder, J.S. Yun, W. Zhang, K.D.G.I. Jayawardena, S.R.P. Silva, Modification of hydrophobic self-assembled monolayers with nanoparticles for improved wettability and enhanced carrier lifetimes over large areas in perovskite solar cells, Sol. RRL 7 (2023) 2300388, https://doi.org/10.1002/solr.202300388.
[87] A. Farag, T. Feeney, I.M. Hossain, F. Schackmar, P. Fassl, K. Küster, R. Bäuerle, M.A. Ruiz-Preciado, M. Hentschel, D.B. Ritzer, A. Diercks, Y. Li, B.A. Nejand, F. Laufer, R. Singh, U. Starke, U.W. Paetzold, Evaporated self-assembled monolayer hole transport layers: lossless interfaces in p-i-n perovskite solar cells, Adv. Energy Mater. 13 (2023) 2203982, https://doi.org/10.1002/aenm.202203982.
[88] K. Hossain, A. Kulkarni, U. Bothra, B. Klingebiel, T. Kirchartz, M. Saliba, D. Kabra, Resolving the hydrophobicity of the Me-4PACz hole transport layer for inverted perovskite solar cells with efficiency >20%, ACS Energy Lett. 8 (2023) 3860–3867, https://doi.org/10.1021/acsenergylett.3c01385.
[89] S.-C. Liu, H.-Y. Lin, S.-E. Hsu, D.-T. Wu, S. Sathasivam, M. Daboczi, H.-J. Hsieh, C.-S. Zeng, T.-G. Hsu, S. Eslava, T.J. Macdonald, C.-T. Lin, Highly reproducible self-assembled monolayer based perovskite solar cells via amphiphilic polyelectrolyte, J. Mater. Chem. A 12 (2024) 2856–2866, https://doi.org/10.1039/D3TA04512A.
[90] X. Zheng, Z. Li, Y. Zhang, M. Chen, T. Liu, C. Xiao, D. Gao, J.B. Patel, D. Kuciauskas, A. Magomedov, R.A. Scheidt, X. Wang, S.P. Harvey, Z. Dai, C. Zhang, D. Morales, H. Pruett, B.M. Wieliczka, A.R. Kirmani, N.P. Padture, K.R. Graham, Y. Yan, M.K. Nazeeruddin, M.D. McGehee, Z. Zhu, J.M. Luther, Co-deposition of hole-selective contact and absorber for improving the processability of perovskite solar cells, Nat. Energy 8 (2023) 462–472, https://doi.org/10.1038/s41560-023-01227-6.
[91] E.J. Cassella, E.L.K. Spooner, T. Thornber, M.E. O'Kane, T.E. Catley, J.E. Bishop, J.A. Smith, O.S. Game, D.G. Lidzey, Gas-assisted spray coating of perovskite solar cells incorporating sprayed self-assembled monolayers, Adv. Sci. 9 (2022) 2104848, https://doi.org/10.1002/advs.202104848.
[92] D. Vidyasagar, Y. Yun, J. Yu Cho, H. Lee, K. Won Kim, Y. Tae Kim, S. Woong Yang, J. Jung, W. Chang Choi, S. Kim, R. Kumar Gunasekaran, S.B. Kang, K. Heo, D.H. Kim, J. Heo, S. Lee, Surface-functionalized hole-selective monolayer for high efficiency single-junction wide-bandgap and monolithic tandem perovskite solar cells, J. Energy Chem. 88 (2024) 317–326, https://doi.org/10.1016/j.jechem.2023.09.023.
[93] D. Song, S. Narra, M.-Y. Li, J.-S. Lin, E.W.-G. Diau, Interfacial engineering with a hole-selective self-assembled monolayer for tin perovskite solar cells via a two-step fabrication, ACS Energy Lett. 6 (2021) 4179–4186, https://doi.org/10.1021/acsenergylett.1c02124.
[94] S. Chen, X. Xiao, B. Chen, L.L. Kelly, J. Zhao, Y. Lin, M.F. Toney, J. Huang, Crystallization in one-step solution deposition of perovskite films: upward or downward? Sci. Adv. 7 (2021) eabb2412 https://doi.org/10.1126/sciadv.abb2412.
[95] R. Mishima, M. Hino, M. Kanematsu, K. Kishimoto, H. Ishibashi, K. Konishi, S. Okamoto, T. Irie, T. Fujimoto, W. Yoshida, H. Uzu, D. Adachi, K. Yamamoto, 28.3% efficient perovskite-silicon tandem solar cells with mixed self-assembled monolayers, Appl. Phys. Express 15 (2022) 076503, https://doi.org/10.35848/1882-0786/ac727b.
[96] M. Wu, X. Li, Z. Ying, Y. Chen, X. Wang, M. Zhang, S. Su, X. Guo, J. Sun, C. Shou, X. Yang, J. Ye, Reconstruction of the indium tin oxide surface enhances the adsorption of high-density self-assembled monolayer for perovskite/silicon tandem solar cells, Adv. Funct. Mater. 33 (2023) 2304708, https://doi.org/10.1002/adfm.202304708.
[97] N. Phung, M. Verheijen, A. Todinova, K. Datta, M. Verhage, A. Al-Ashouri, H. Köbler, X. Li, A. Abate, S. Albrecht, M. Creatore, Enhanced self-assembled monolayer surface coverage by ALD NiO in p-i-n perovskite solar cells, ACS Appl.

Mater. Interfaces 14 (2022) 2166–2176, https://doi.org/10.1021/acsami.1c15860.
[98] K. Almasabi, X. Zheng, B. Turedi, A.Y. Alsalloum, M.N. Lintangpradipto, J. Yin, L. Gutiérrez-Arzaluz, K. Kotsovos, A. Jamal, I. Gereige, O.F. Mohammed, O.M. Bakr, Hole-transporting self-assembled monolayer enables efficient single-crystal perovskite solar cells with enhanced stability, ACS Energy Lett. 8 (2023) 950–956, https://doi.org/10.1021/acsenergylett.2c02333.
[99] R. Azmi, D.S. Utomo, B. Vishal, S. Zhumagali, P. Dally, A.M. Risqi, A. Prasetio, E. Ugur, F. Cao, I.F. Imran, A.A. Said, A.R. Pininti, A.S. Subbiah, E. Aydin, C. Xiao, S.I. Seok, S. De Wolf, Double-side 2D/3D heterojunctions for inverted perovskite solar cells, Nature 628 (2024) 93–98, https://doi.org/10.1038/s41586-024-07189-3.
[100] K. Datta, J. Wang, D. Zhang, V. Zardetto, W.H.M. Remmerswaal, C.H.L. Weijtens, M.M. Wienk, R.A.J. Janssen, Monolithic all-perovskite tandem solar cells with minimized optical and energetic losses, Adv. Mater. 34 (2022) 2110053, https://doi.org/10.1002/adma.202110053.
[101] H. Lai, J. Luo, Y. Zwirner, S. Olthof, A. Wieczorek, F. Ye, Q. Jeangros, X. Yin, F. Akhundova, T. Ma, R. He, R.K. Kothandaraman, X. Chin, E. Gilshtein, A. Müller, C. Wang, J. Thiesbrummel, S. Siol, J.M. Prieto, T. Unold, M. Stolterfoht, C. Chen, A.N. Tiwari, D. Zhao, F. Fu, High-performance flexible all-perovskite tandem solar cells with reduced V_{OC}-deficit in wide-bandgap subcell, Adv. Energy Mater. 12 (2022) 2202438, https://doi.org/10.1002/aenm.202202438.
[102] J. Zeng, L. Bi, Y. Cheng, B. Xu, A.K.Y. Jen, Self-assembled monolayer enabling improved buried interfaces in blade-coated perovskite solar cells for high efficiency and stability, Nano Res. Energy 1 (2022) 9120004, https://doi.org/10.26599/NRE.2022.9120004.
[103] Y. Wu, Z. Huang, Q. Li, C. Yang, S. Zhan, X. Jia, C. Li, M.R. Islam, Z. Wang, S. Yue, K. Liu, S. Qu, Comprehensively evaluating feasibility of self-assembled materials applied to hole transport layer for commercializing perovskite solar cells, Mater. Res. Bull. 165 (2023) 112327, https://doi.org/10.1016/j.materresbull.2023.112327.
[104] S.K. Hau, Y.-J. Cheng, H.-L. Yip, Y. Zhang, H. Ma, A.K.Y. Jen, Effect of chemical modification of fullerene-based self-assembled monolayers on the performance of inverted polymer solar cells, ACS Appl. Mater. Interfaces 2 (2010) 1892–1902, https://doi.org/10.1021/am100238e.
[105] A. Abrusci, S.D. Stranks, P. Docampo, H.-L. Yip, A.K.Y. Jen, H.J. Snaith, High-performance perovskite-polymer hybrid solar cells via electronic coupling with fullerene monolayers, Nano Lett. 13 (2013) 3124–3128, https://doi.org/10.1021/nl401044q.
[106] K. Wojciechowski, S.D. Stranks, A. Abate, G. Sadoughi, A. Sadhanala, N. Kopidakis, G. Rumbles, C.-Z. Li, R.H. Friend, A.K.Y. Jen, H.J. Snaith, Heterojunction modification for highly efficient organic–inorganic perovskite solar cells, ACS Nano 8 (2014) 12701–12709, https://doi.org/10.1021/nn505723h.
[107] M. Valles-Pelarda, B.C. Hames, I. García-Benito, O. Almora, A. Molina-Ontoria, R.S. Sánchez, G. Garcia-Belmonte, N. Martín, I. Mora-Sero, Analysis of the hysteresis behavior of perovskite solar cells with interfacial fullerene self-assembled monolayers, J. Phys. Chem. Lett. 7 (2016) 4622–4628, https://doi.org/10.1021/acs.jpclett.6b02103.
[108] G. Tumen-Ulzii, T. Matsushima, D. Klotz, M.R. Leyden, P. Wang, C. Qin, J.-W. Lee, S.-J. Lee, Y. Yang, C. Adachi, Hysteresis-less and stable perovskite solar cells with a self-assembled monolayer, Commun. Mater. 1 (2020) 31, https://doi.org/10.1038/s43246-020-0028-z.
[109] S. Zhang, M. Li, H. Zeng, X. Zheng, L. Luo, S. You, Y. Zhao, R. Liu, C. Tian, X. Li, Grain boundary and buried interface suturing enabled by fullerene derivatives for high-performance perovskite solar module, ACS Energy Lett. 7 (2022) 3958–3966, https://doi.org/10.1021/acsenergylett.2c01854.
[110] T. Leijtens, G.E. Eperon, S. Pathak, A. Abate, M.M. Lee, H.J. Snaith, Overcoming ultraviolet light instability of sensitized TiO_2 with meso-superstructured organometal tri-halide perovskite solar cells, Nat. Commun. 4 (2013) 2885, https://doi.org/10.1038/ncomms3885.
[111] J. Yang, B.D. Siempelkamp, E. Mosconi, F. De Angelis, T.L. Kelly, Origin of the thermal instability in $CH_3NH_3PbI_3$ thin films deposited on ZnO, Chem. Mater. 27 (2015) 4229–4236, https://doi.org/10.1021/acs.chemmater.5b01598.
[112] Q. Jiang, L. Zhang, H. Wang, X. Yang, J. Meng, H. Liu, Z. Yin, J. Wu, X. Zhang, J. You, Enhanced electron extraction using SnO_2 for high-efficiency planar-structure $HC(NH_2)_2PbI_3$-based perovskite solar cells, Nat. Energy 2 (2016) 16177, https://doi.org/10.1038/nenergy.2016.177.
[113] H. Zhang, C. Zhao, J. Yao, W.C.H. Choy, Dopant-free NiO_x nanocrystals: a low-cost and stable hole transport material for commercializing perovskite optoelectronics, Angew. Chem. Int. Ed. 62 (2023) e202219307, https://doi.org/10.1002/anie.202219307.
[114] C.C. Boyd, R.C. Shallcross, T. Moot, R. Kerner, L. Bertoluzzi, A. Onno, S. Kavadiya, C. Chosy, E.J. Wolf, J. Werner, J.A. Raiford, C. de Paula, A.F. Palmstrom, Z.J. Yu, J.J. Berry, S.F. Bent, Z.C. Holman, J.M. Luther, E.L. Ratcliff, N.R. Armstrong, M.D. McGehee, Overcoming redox reactions at perovskite-nickel oxide interfaces to boost voltages in perovskite solar cells, Joule 4 (2020) 1759–1775, https://doi.org/10.1016/j.joule.2020.06.004.
[115] M. Li, Z. Zhang, J. Sun, F. Liu, J. Chen, L. Ding, C. Chen, Perovskite solar cells with NiOx hole-transport layer, J. Semicond. 44 (2023) 100201, https://doi.org/10.1088/1674-4926/44/10/100201.
[116] Y. Ogomi, A. Morita, S. Tsukamoto, T. Saitho, Q. Shen, T. Toyoda, K. Yoshino, S.S. Pandey, T. Ma, S. Hayase, All-solid perovskite solar cells with HOCO-R-$NH_3^+I^-$ anchor-group inserted between porous titania and perovskite, J. Phys. Chem. C 118 (2014) 16651–16659, https://doi.org/10.1021/jp412627n.
[117] J. Cao, J. Yin, S. Yuan, Y. Zhao, J. Li, N. Zheng, Thiols as interfacial modifiers to enhance the performance and stability of perovskite solar cells, Nanoscale 7 (2015) 9443–9447, https://doi.org/10.1039/C5NR01820J.
[118] L. Liu, A. Mei, T. Liu, P. Jiang, Y. Sheng, L. Zhang, H. Han, Fully printable mesoscopic perovskite solar cells with organic silane self-assembled monolayer, J. Am. Chem. Soc. 137 (2015) 1790–1793, https://doi.org/10.1021/ja5125594.
[119] B. Li, Y. Chen, Z. Liang, D. Gao, W. Huang, Interfacial engineering by using self-assembled monolayer in mesoporous perovskite solar cell, RSC Adv. 5 (2015) 94290–94295, https://doi.org/10.1039/C5RA17129F.
[120] Ç. Kırbıyık, K. Kara, D.A. Kara, M.Z. Yiğit, B. İstanbullu, M. Can, N.S. Sariciftci, M. Scharber, M. Kuş, Enhancing the c-TiO2 based perovskite solar cell performance via modification by a serial of boronic acid derivative self-assembled monolayers, Appl. Surf. Sci. 423 (2017) 521–527, https://doi.org/10.1016/j.apsusc.2017.06.189.
[121] F. Han, Z. Tu, Z. Wan, J. Luo, J. Xia, G. Hao, Y. Yi, R. Wang, C. Jia, Effect of functional group position change of pyridinesulfonic acid as interface-modified layer on perovskite solar cell, Appl. Surf. Sci. 462 (2018) 517–525, https://doi.org/10.1016/j.apsusc.2018.08.088.
[122] H. Lu, J. Zhuang, Z. Ma, Y. Deng, Q. Wang, Z. Guo, S. Zhao, H. Li, γ-MPTS-SAM modified meso-TiO_2 surface to enhance performance in perovskite solar cell, Mater. Sci. Semicond. Process. 97 (2019) 21–28, https://doi.org/10.1016/j.mssp.2019.02.018.
[123] R. Zhang, W. Liu, R. Hu, Y. Ma, Y. Sun, J. Zhang, Y. Pu, J. Yang, L. Chu, X.a. Li, Enhancing perovskite quality and energy level alignment of TiO_2 nanorod arrays-based solar cells via interfacial modification, Sol. Energy Mater. Sol. Cells 191 (2019) 183–189, https://doi.org/10.1016/j.solmat.2018.11.006.
[124] F. Han, G. Hao, Z. Wan, J. Luo, J. Xia, C. Jia, Bifunctional electron transporting layer/perovskite interface linker for highly efficient perovskite solar cells, Electrochim. Acta 296 (2019) 75–81, https://doi.org/10.1016/j.electacta.2018.10.130.
[125] S.Y. Abate, D.-C. Huang, Y.-T. Tao, Surface modification of TiO_2 layer with phosphonic acid monolayer in perovskite solar cells: effect of chain length and terminal functional group, Org. Electron. 78 (2020) 105583, https://doi.org/10.1016/j.orgel.2019.105583.
[126] T. Liu, X. Zhao, X. Zhong, Q.C. Burlingame, A. Kahn, Y.-L. Loo, Improved absorber phase stability, performance, and lifetime in inorganic perovskite solar cells with alkyltrimethoxysilane strain-release layers at the perovskite/TiO_2 interface, ACS Energy Lett. 7 (2022) 3531–3538, https://doi.org/10.1021/acsenergylett.2c01610.
[127] I.S. Yang, Z. Dai, A. Ranka, D. Chen, K. Zhu, J.J. Berry, P. Guo, N.P. Padture, Simultaneous enhancement of efficiency and operational-stability of mesoscopic perovskite solar cells via interfacial toughening, Adv. Mater. 36 (2024) 2308819, https://doi.org/10.1002/adma.202308819.
[128] L. Zuo, Z. Gu, T. Ye, W. Fu, G. Wu, H. Li, H. Chen, Enhanced photovoltaic performance of $CH_3NH_3PbI_3$ perovskite solar cells through interfacial engineering using self-assembling monolayer, J. Am. Chem. Soc. 137 (2015) 2674–2679, https://doi.org/10.1021/ja512518r.
[129] Q. An, P. Fassl, Y.J. Hofstetter, D. Becker-Koch, A. Bausch, P.E. Hopkinson, Y. Vaynzof, High performance planar perovskite solar cells by ZnO electron transport layer engineering, Nano Energy 39 (2017) 400–408, https://doi.org/10.1016/j.nanoen.2017.07.013.
[130] R. Azmi, C.-L. Lee, I.H. Jung, S.-Y. Jang, Simultaneous improvement in efficiency and stability of low-temperature-processed perovskite solar cells by interfacial control, Adv. Energy Mater. 8 (2018) 1702934, https://doi.org/10.1002/aenm.201702934.
[131] R. Azmi, W.T. Hadmojo, S. Sinaga, C.-L. Lee, S.C. Yoon, I.H. Jung, S.-Y. Jang, High-efficiency low-temperature ZnO based perovskite solar cells based on highly polar, nonwetting self-assembled molecular layers, Adv. Energy Mater. 8 (2018) 1701683, https://doi.org/10.1002/aenm.201701683.
[132] J. Han, H. Kwon, E. Kim, D.-W. Kim, H.J. Son, D.H. Kim, Interfacial engineering of a ZnO electron transporting layer using self-assembled monolayers for high performance and stable perovskite solar cells, J. Mater. Chem. A 8 (2020) 2105–2113, https://doi.org/10.1039/C9TA12750J.
[133] C. Liu, D. Zhang, Z. Li, W. Han, G. Ren, Z. Li, L. Shen, W. Guo, W. Zheng, Incorporating a polar molecule to passivate defects for perovskite solar cells, Sol. RRL 4 (2020) 1900489, https://doi.org/10.1002/solr.201900489.
[134] H. Kouki, S. Pitié, A. Torkhani, F. Mamèche, P. Decorse, M. Seydou, F. Kouki, P. Lang, Tailor-made amino-based self-assembled monolayers grafted on electron transport ZnO layers: perovskite solar cell performance and modified interface relationship, ACS Appl. Energy Mater. 5 (2022) 1635–1645, https://doi.org/10.1021/acsaem.1c03050.
[135] Y. Wu, J. Song, X. Wu, C. Qiu, X. Yin, L. Hu, Z. Su, Y. Jin, J. Chen, Z. Li, Highly efficient and stable ZnO-based perovskite solar cells enabled by a self-assembled monolayer as the interface linker, Chem. Commun. 58 (2022) 9266–9269, https://doi.org/10.1039/D2CC03890K.
[136] L. Zuo, Q. Chen, N. De Marco, Y.-T. Hsieh, H. Chen, P. Sun, S.-Y. Chang, H. Zhao, S. Dong, Y. Yang, Tailoring the interfacial chemical interaction for high-efficiency perovskite solar cells, Nano Lett. 17 (2017) 269–275, https://doi.org/10.1021/acs.nanolett.6b04015.
[137] G. Yang, C. Wang, H. Lei, X. Zheng, P. Qin, L. Xiong, X. Zhao, Y. Yan, G. Fang, Interface engineering in planar perovskite solar cells: energy level alignment, perovskite morphology control and high performance achievement, J. Mater. Chem. A 5 (2017) 1658–1666, https://doi.org/10.1039/C6TA08783C.
[138] M. Hou, H. Zhang, Z. Wang, Y. Xia, Y. Chen, W. Huang, Enhancing efficiency and stability of perovskite solar cells via a self-assembled dopamine interfacial layer,

ACS Appl. Mater. Interfaces 10 (2018) 30607–30613, https://doi.org/10.1021/acsami.8b10332.
[139] J. Du, L. Feng, X. Guo, X. Huang, Z. Lin, J. Su, Z. Hu, J. Zhang, J. Chang, Y. Hao, Enhanced efficiency and stability of planar perovskite solar cells by introducing amino acid to SnO_2/perovskite interface, J. Power Sources 455 (2020) 227974, https://doi.org/10.1016/j.jpowsour.2020.227974.
[140] G.-W. Kim, Y. Choi, H. Choi, J. Min, T. Park, S. Song, Novel cathode interfacial layer using creatine for enhancing the photovoltaic properties of perovskite solar cells, J. Mater. Chem. A 8 (2020) 21721–21728, https://doi.org/10.1039/D0TA08239B.
[141] J. Yan, Z. Lin, Q. Cai, X. Wen, C. Mu, Choline chloride-modified SnO_2 achieving high output voltage in $MAPbI_3$ perovskite solar cells, ACS Appl. Energy Mater. 3 (2020) 3504–3511, https://doi.org/10.1021/acsaem.0c00038.
[142] Z. Dai, S.K. Yadavalli, M. Chen, A. Abbaspourtamijani, Y. Qi, N.P. Padture, Interfacial toughening with self-assembled monolayers enhances perovskite solar cell reliability, Science 372 (2021) 618–622, https://doi.org/10.1126/science.abf5602.
[143] H. Dong, G. Shen, Z. Lin, Q. Cai, Y. Li, X. Xu, W. Zhang, C. Mu, Bifunctional interfacial regulation with 4-(trifluoromethyl) benzoic acid to reduce the photovoltage deficit of $MAPbI_3$-based perovskite solar cells, ChemNanoMat 8 (2022) e202100475, https://doi.org/10.1002/cnma.202100475.
[144] B. Li, C. Zhang, D. Gao, X. Sun, S. Zhang, Z. Li, J. Gong, S. Li, Z. Zhu, Suppressing oxidation at perovskite-NiO_x interface for efficient and stable tin perovskite solar cells, Adv. Mater. 36 (2024) e2309768, https://doi.org/10.1002/adma.202309768.
[145] X. Sun, H. Jiang, Y. Sun, Z. Guo, Z. Pang, F. Wang, J. Yang, L. Yang, Multi-functional L-histidine self-assembled monolayers on SnO_2 electron transport layer to boost photovoltaic performance of perovskite solar cells, Electrochim. Acta 428 (2022) 140930, https://doi.org/10.1016/j.electacta.2022.140930.
[146] X. Zuo, B. Kim, B. Liu, D. He, L. Bai, W. Wang, C. Xu, Q. Song, C. Jia, Z. Zang, D. Lee, X. Li, J. Chen, Passivating buried interface via self-assembled novel sulfonium salt toward stable and efficient perovskite solar cells, Chem. Eng. J. 431 (2022) 133209, https://doi.org/10.1016/j.cej.2021.133209.
[147] L. Yang, H. Zhou, Y. Duan, M. Wu, K. He, Y. Li, D. Xu, H. Zou, S. Yang, Z. Fang, S. Liu, Z. Liu, 25.24%-Efficiency $FACsPbI_3$ perovskite solar cells enabled by intermolecular esterification reaction of DL-carnitine hydrochloride, Adv. Mater 35 (2023) 2211545, https://doi.org/10.1002/adma.202211545.
[148] Z. Yi, X. Li, B. Xiao, Q. Jiang, Y. Luo, J. Yang, Dual-interface engineering induced by silane coupling agents with different functional groups constructing high-performance flexible perovskite solar cells, Chem. Eng. J. 469 (2023) 143790, https://doi.org/10.1016/j.cej.2023.143790.
[149] L. Yin, C. Ding, C. Liu, C. Zhao, W. Zha, I.Z. Mitrovic, E.G. Lim, Y. Han, X. Gao, L. Zhang, H. Wang, Y. Li, S. Wilken, R. Österbacka, H. Lin, C.-Q. Ma, C. Zhao, A multifunctional molecular bridging layer for high efficiency, hysteresis-free, and stable perovskite solar cells, Adv. Energy Mater. 13 (2023) 2301161, https://doi.org/10.1002/aenm.202301161.
[150] X. Zhuang, D. Ma, G. Li, Z. Yang, Z. Zhang, J. Zhao, Z. Chi, Size-matched dicarboxylic acid for buried interfacial engineering in high-performance perovskite solar cells, Chem. Eng. J. 460 (2023) 141705, https://doi.org/10.1016/j.cej.2023.141705.
[151] C. Zhang, Y. Son, H. Kim, S.-H. Lee, X. Liang, G. Fu, S.-U. Lee, D.-A. Park, Q. Jiang, K. Zhu, N.-G. Park, Work function tuning of a weak adhesion homojunction for stable perovskite solar cells, Joule 8 (2024) 1394–1411, https://doi.org/10.1016/j.joule.2024.02.015.
[152] Q. Wang, C.-C. Chueh, T. Zhao, J. Cheng, M. Eslamian, W.C.H. Choy, A.K.-Y. Jen, Effects of self-assembled monolayer modification of nickel oxide nanoparticles layer on the performance and application of inverted perovskite solar cells, ChemSusChem 10 (2017) 3794–3803, https://doi.org/10.1002/cssc.201701262.
[153] J. Mangalam, T. Rath, S. Weber, B. Kunert, T. Dimopoulos, A. Fian, G. Trimmel, Modification of NiO_x hole transport layers with 4-bromobenzylphosphonic acid and its influence on the performance of lead halide perovskite solar cells, J. Mater. Sci. Mater. Electron. 30 (2019) 9602–9611, https://doi.org/10.1007/s10854-019-01294-0.
[154] H. Anizelli, T.W. David, P. Tyagi, E. Laureto, J. Kettle, Enhancing the stability of perovskite solar cells through functionalisation of metal oxide transport layers with self-assembled monolayers, Sol. Energy 203 (2020) 157–163, https://doi.org/10.1016/j.solener.2020.04.035.
[155] N. Singh, Y.-T. Tao, Effect of surface modification of nickel oxide hole-transport layer via self-assembled monolayers in perovskite solar cells, Nano Select 2 (2021) 2390–2399, https://doi.org/10.1002/nano.202100004.
[156] H. Liu, K. Yan, J. Rao, Z. Chen, B. Niu, Y. Huang, H. Ju, B. Yan, J. Yao, H. Zhu, H. Chen, C.-Z. Li, Self-assembled donor–acceptor dyad molecules stabilize the heterojunction of inverted perovskite solar cells and modules, ACS Appl. Mater. Interfaces 14 (2022) 6794–6800, https://doi.org/10.1021/acsami.1c22396.
[157] J. Zhang, J. Yang, R. Dai, W. Sheng, Y. Su, Y. Zhong, X. Li, L. Tan, Y. Chen, Elimination of interfacial lattice mismatch and detrimental reaction by self-assembled layer dual-passivation for efficient and stable inverted perovskite solar cells, Adv. Energy Mater. 12 (2022) 2103674, https://doi.org/10.1002/aenm.202103674.
[158] L. Li, Y. Wang, X. Wang, R. Lin, X. Luo, Z. Liu, K. Zhou, S. Xiong, Q. Bao, G. Chen, Y. Tian, Y. Deng, K. Xiao, J. Wu, M.I. Saidaminov, H. Lin, C.-Q. Ma, Z. Zhao, Y. Wu, L. Zhang, H. Tan, Flexible all-perovskite tandem solar cells approaching 25% efficiency with molecule-bridged hole-selective contact, Nat. Energy 7 (2022) 708–717, https://doi.org/10.1038/s41560-022-01045-2.
[159] S. Yu, Z. Xiong, H. Zhou, Q. Zhang, Z. Wang, F. Ma, Z. Qu, Y. Zhao, X. Chu, X. Zhang, J. You, Homogenized NiO_x nanoparticles for improved hole transport in inverted perovskite solar cells, Science 382 (2023) 1399–1404, https://doi.org/10.1126/science.adj8858.
[160] B. Niu, H. Liu, Y. Huang, E. Gu, M. Yan, Z. Shen, K. Yan, B. Yan, J. Yao, Y. Fang, H. Chen, C.-Z. Li, Multifunctional hybrid interfacial layers for high-performance inverted perovskite solar cells, Adv. Mater. 35 (2023) 2212258, https://doi.org/10.1002/adma.202212258.
[161] H. Bian, J. You, C. Xu, X. He, M. Wang, Y. Yao, W. Zeng, P. Guo, H. Zhou, D. Lu, Z. Dai, S. Zhang, Q. Song, Chemically suppressing redox reaction at the NiO_x/perovskite interface in narrow bandgap perovskite solar cells to exceed a power conversion efficiency of 20%, J. Mater. Chem. A 11 (2023) 205–212, https://doi.org/10.1039/D2TA06211A.
[162] Z. Li, X. Sun, X. Zheng, B. Li, D. Gao, S. Zhang, X. Wu, S. Li, J. Gong, J.M. Luther, Z.a. Li, Z. Zhu, Stabilized hole-selective layer for high-performance inverted p-i-n perovskite solar cells, Science 382 (2023) 284–289, https://doi.org/10.1126/science.ade9637.
[163] L. Li, M. Wei, V. Carnevali, H. Zeng, M. Zeng, R. Liu, N. Lempesis, F.T. Eickemeyer, L. Luo, L. Agosta, M. Dankl, S.M. Zakeeruddin, U. Roethlisberger, M. Gratzel, Y. Rong, X. Li, Buried-interface engineering enables efficient and 1960-hour ISOS-L-2I stable inverted perovskite solar cells, Adv. Mater. 36 (2024) e2303869, https://doi.org/10.1002/adma.202303869.
[164] B. Nath, S.K. Behera, J. Kumar, A. Hemmerle, P. Fontaine, P.C. Ramamurthy, D.R. Mahapatra, G. Hegde, Understanding the heterointerfaces in perovskite solar cells via hole selective layer surface functionalization, Adv. Mater. 36 (2024) e2307547, https://doi.org/10.1002/adma.202307547.
[165] L. Cao, Y. Tong, Y. Ke, W. Zhang, T. Li, Z. Kang, H. Wang, K. Wang, Modification of nickel oxide via self-assembled monolayer for enhanced performance of air-processed $FAPbI_3$ perovskite solar cells, ACS Appl. Energy Mater. 7 (2024) 1508–1516, https://doi.org/10.1021/acsaem.3c02777.
[166] Q. Cao, T. Wang, X. Pu, X. He, M. Xiao, H. Chen, L. Zhuang, Q. Wei, H.L. Loi, P. Guo, B. Kang, G. Feng, J. Zhuang, G. Feng, X. Li, F. Yan, Co-Self-Assembled monolayers modified NiO_x for stable inverted perovskite solar cells, Adv. Mater. 36 (2024) e2311970, https://doi.org/10.1002/adma.202311970.
[167] G. Kim, H. Kim, M. Kim, J. Sin, M. Kim, J. Kim, H. Zhou, S.H. Kang, H.M. Oh, J. Yang, Enhancing surface modification and carrier extraction in inverted perovskite solar cells via self-assembled monolayers, Nanomater 14 (2024) 214, https://doi.org/10.3390/nano14020214.
[168] X. Yuan, X. Ling, H. Wang, C. Shen, R. Li, Y. Deng, S. Chen, Modulation on electrostatic potential to build a firm bridge at NiO_x/perovskite interface for efficient and stable perovskite solar cells, J. Energy Chem. 96 (2024) 249–258, https://doi.org/10.1016/j.jechem.2024.04.036.
[169] Y. Zhou, X.Z. Huang, J.S. Zhang, L. Zhang, H.T. Wu, Y. Zhou, Y. Wang, Y. Wang, W.F. Fu, H.Z. Chen, Interfacial modification of NiO_x for highly efficient and stable inverted perovskite solar cells, Adv. Energy Mater. 14 (2024) 2400616, https://doi.org/10.1002/aenm.202400616.
[170] B. Li, P. Wang, M. Shao, J. Bao, X. Wu, P. Lin, L. Xu, X. Yu, C. Cui, Multifunctional zwitterion modified SnO_2 nanoparticles for efficient and stable planar perovskite solar cells, Org. Electron. 106 (2022) 106519, https://doi.org/10.1016/j.orgel.2022.106519.
[171] Z. Gu, L. Zuo, T.T. Larsen-Olsen, T. Ye, G. Wu, F.C. Krebs, H. Chen, Interfacial engineering of self-assembled monolayer modified semi-roll-to-roll planar heterojunction perovskite solar cells on flexible substrates, J. Mater. Chem. A. 3 (2015) 24254–24260, https://doi.org/10.1039/C5TA07008B.
[172] W.F. Fu, A.G. Ricciardulli, Q.A. Akkerman, R.A. John, M.M. Tavakoli, S. Essig, M.V. Kovalenko, M. Saliba, Stability of perovskite materials and devices, Mater. Today 58 (2022) 275–296, https://doi.org/10.1016/j.mattod.2022.06.020.
[173] F. Wang, S. Bai, W. Tress, A. Hagfeldt, F. Gao, Defects engineering for high-performance perovskite solar cells, npj Flex. Electron. 2 (2018) 22, https://doi.org/10.1038/s41528-018-0035-z.
[174] S. Chen, Y. Liu, X. Xiao, Z. Yu, Y. Deng, X. Dai, Z. Ni, J. Huang, Identifying the soft nature of defective perovskite surface layer and its removal using a facile mechanical approach, Joule 4 (2020) 2661–2674, https://doi.org/10.1016/j.joule.2020.10.014.
[175] M. Kedia, M. Rai, H. Phirke, C.A. Aranda, C. Das, V. Chirvony, S. Boehringer, M. Kot, M.M. Byranvand, J.I. Flege, A. Redinger, M. Saliba, Light makes right: laser polishing for surface modification of perovskite solar cells, ACS Energy Lett. 8 (2023) 2603–2610, https://doi.org/10.1021/acsenergylett.3c00469.
[176] C. Xu, L. Zuo, P. Hang, X. Guo, Y. Pan, G. Zhou, T. Chen, B. Niu, X. Xu, Z. Hong, D. Wang, H. Zhu, X. Yu, D. Yang, H. Chen, Synergistic effects of bithiophene ammonium salt for high-performance perovskite solar cells, J. Mater. Chem. A 10 (2022) 9971–9980, https://doi.org/10.1039/D2TA01349E.
[177] G. Wu, R. Liang, M. Ge, G. Sun, Y. Zhang, G. Xing, Surface passivation using 2D perovskites toward efficient and stable perovskite solar cells, Adv. Mater. 34 (2022) 2105635, https://doi.org/10.1002/adma.202105635.
[178] S.M. Park, M. Wei, J. Xu, H.R. Atapattu, F.T. Eickemeyer, K. Darabi, L. Grater, Y. Yang, C. Liu, S. Teale, B. Chen, H. Chen, T. Wang, L. Zeng, A. Maxwell, Z. Wang, K.R. Rao, Z. Cai, S.M. Zakeeruddin, J.T. Pham, C.M. Risko, A. Amassian, M.G. Kanatzidis, K.R. Graham, M. Grätzel, E.H. Sargent, Engineering ligand reactivity enables high-temperature operation of stable perovskite solar cells, Science 381 (2023) 209–215, https://doi.org/10.1126/science.adi4107.
[179] J. Zhang, Z. Hu, L. Huang, G. Yue, J. Liu, X. Lu, Z. Hu, M. Shang, L. Han, Y. Zhu, Bifunctional alkyl chain barriers for efficient perovskite solar cells, Chem. Commun. 51 (2015) 7047–7050, https://doi.org/10.1039/C5CC00128E.
[180] Q. Li, Y. Zheng, X. Guo, G. Zhang, G. Ding, Y. Shi, F. Li, M. Sun, Y. Shao, Interface engineering enhances the photovoltaic performance of wide bandgap $FAPbBr_3$ perovskite for application in low-light environments, Adv. Funct. Mater. 33 (2023) 2303729, https://doi.org/10.1002/adfm.202303729.

[181] Q. Wang, Q. Dong, T. Li, A. Gruverman, J. Huang, Thin insulating tunneling contacts for efficient and water-resistant perovskite solar cells, Adv. Mater. 28 (2016) 6734–6739, https://doi.org/10.1002/adma.201600969.
[182] H. Xiong, Y. Rui, Y. Li, Q. Zhang, H. Wang, Hydrophobic coating over a $CH_3NH_3PbI_3$ absorbing layer towards air stable perovskite solar cells, J. Mater. Chem. C 4 (2016) 6848–6854, https://doi.org/10.1039/C6TC02238C.
[183] N. Perumbalathodi, T.-S. Su, Z.-F. He, K. Kannankutty, T.-C. Wei, Bidirectional passivation for highly efficient and stable CuSCN-based perovskite solar cells using (3-mercaptopropyl)trimethoxysilane, ACS Appl. Energy Mater. 7 (2024) 3656–3666, https://doi.org/10.1021/acsaem.3c03190.
[184] L. Xie, J. Chen, P. Vashishtha, X. Zhao, G.S. Shin, S.G. Mhaisalkar, N.-G. Park, Importance of functional groups in cross-linking methoxysilane additives for high-efficiency and stable perovskite solar cells, ACS Energy Lett. 4 (2019) 2192–2200, https://doi.org/10.1021/acsenergylett.9b01356.
[185] B. Wang, H. Li, Q. Dai, M. Zhang, Z. Zou, J.-L. Brédas, Z. Lin, Robust molecular dipole-enabled defect passivation and control of energy-level alignment for high-efficiency perovskite solar cells, Angew. Chem. Int. Ed. 60 (2021) 17664–17670, https://doi.org/10.1002/anie.202105512.
[186] Y. Shi, E. Rojas-Gatjens, J. Wang, J. Pothoof, R. Giridharagopal, K. Ho, F. Jiang, M. Taddei, Z. Yang, E.M. Sanehira, M.D. Irwin, C. Silva-Acuña, D.S. Ginger, (3-Aminopropyl)trimethoxysilane surface passivation improves perovskite solar cell performance by reducing surface recombination velocity, ACS Energy Lett. 7 (2022) 4081–4088, https://doi.org/10.1021/acsenergylett.2c01766.
[187] A.I.A. Soliman, Y.Q. Zhang, L. Zhang, H.T. Wu, S.Q. Shan, Y. Zhou, C. Xu, W.F. Fu, H.Z. Chen, Surface reconstruction of perovskites with organosilanes for high performance and highly stable solar cells, Adv. Funct. Mater. (2024) 2412886, https://doi.org/10.1002/adfm.202412886.
[188] C.M. Wolff, L. Canil, C. Rehermann, N. Ngoc Linh, F. Zu, M. Ralaiarisoa, P. Caprioglio, L. Fiedler, M. Stolterfoht, S. Kogikoski Jr., I. Bald, N. Koch, E.L. Unger, T. Dittrich, A. Abate, D. Neher, Perfluorinated self-assembled monolayers enhance the stability and efficiency of inverted perovskite solar cells, ACS Nano 14 (2020) 1445–1456, https://doi.org/10.1021/acsnano.9b03268.
[189] H. Zhang, K. Li, M. Sun, F. Wang, H. Wang, A.K.-Y. Jen, Design of superhydrophobic surfaces for stable perovskite solar cells with reducing lead leakage, Adv. Energy Mater. 11 (2021) 2102281, https://doi.org/10.1002/aenm.202102281.
[190] G. Wang, C. Wang, Y. Gao, S. Wen, R.C.I. MacKenzie, L. Guo, W. Dong, S. Ruan, Passivation agent with dipole moment for surface modification towards efficient and stable perovskite solar cells, J. Energy Chem. 64 (2022) 55–61, https://doi.org/10.1016/j.jechem.2021.04.023.
[191] L. Liu, Y. Yang, M. Du, Y. Cao, X. Ren, L. Zhang, H. Wang, S. Zhao, K. Wang, S. Liu, Self-assembled amphiphilic monolayer for efficient and stable wide-bandgap perovskite solar cells, Adv. Energy Mater. 13 (2023) 2202802, https://doi.org/10.1002/aenm.202202802.
[192] H. Guo, X. Wang, C. Li, H. Hu, H. Zhang, L. Zhang, W.-H. Zhu, Y. Wu, Immobilizing surface halide in perovskite solar cells via calix[4]pyrrole, Adv. Mater. 35 (2023) 2301871, https://doi.org/10.1002/adma.202301871.
[193] J. Chen, X. Zhang, X. Liu, B. Li, M. Han, S. Han, Y. Han, J. Liu, W. Dai, R. Ghadari, S. Dai, A multifunctional dye molecule as the interfacial layer for perovskite solar cells, ACS Appl. Mater. Interfaces 16 (2024) 22079–22088, https://doi.org/10.1021/acsami.4c03383.
[194] X. Wang, Y. Zhong, X. Luo, W. Sheng, J. Yang, L. Tan, Y. Chen, Elimination of charge accumulation by a self-assembled cocrystal interlayer for efficient and stable perovskite solar cells, Energy Environ. Sci. 17 (2024) 569–579, https://doi.org/10.1039/D3EE03550F.
[195] J. Liu, J. Chen, L. Xie, S. Yang, Y. Meng, M. Li, C. Xiao, J. Zhu, H. Do, J. Zhang, M. Yang, Z. Ge, Alkyl chains tune molecular orientations to enable dual passivation in inverted perovskite solar cells, Angew. Chem. Int. Ed. 63 (2024) e202403610, https://doi.org/10.1002/anie.202403610.
[196] C. Zhou, Y. Xu, Y. Li, K. Du, X. Li, X. Dong, L. Li, N. Yuan, J. Ding, Flexible perovskite solar cells on ultra-thin stainless-steel with a power-to-weight ratio over 3000 W kg^{-1}, Sol. RRL 8 (2024) 2300901, https://doi.org/10.1002/solr.202300901.
[197] N. Mussakhanuly, E. Choi, R. L Chin, Y. Wang, J. Seidel, M.A. Green, A. M Soufiani, X. Hao, J.S. Yun, Multifunctional surface treatment against imperfections and halide segregation in wide-band gap perovskite solar cells, ACS Appl. Mater. Interfaces 16 (2024) 7961–7972, https://doi.org/10.1021/acsami.3c12616.
[198] H. Chen, C. Liu, J. Xu, A. Maxwell, W. Zhou, Y. Yang, Q. Zhou, A.S.R. Bati, H. Wan, Z. Wang, L. Zeng, J. Wang, P. Serles, Y. Liu, S. Teale, Y. Liu, M.I. Saidaminov, M. Li, N. Rolston, S. Hoogland, T. Filleter, M.G. Kanatzidis, B. Chen, Z. Ning, E.H. Sargent, Improved charge extraction in inverted perovskite solar cells with dual-site-binding ligands, Science 384 (2024) 189–193, https://doi.org/10.1126/science.adm9474.
[199] T. Xu, W. Xiang, X. Ru, Z. Wang, Y. Liu, N. Li, H. Xu, S. Liu, Enhancing stability and efficiency of inverted inorganic perovskite solar cells with in-situ interfacial cross-linked modifier, Adv. Mater. 36 (2024) 2312237, https://doi.org/10.1002/adma.202312237.
[200] D. Zhu, Y. Guo, C. Mu, Z. Jin, S. Yuan, Y. Qin, J.-P. Zhang, X.-C. Ai, Bifunctional chlorosilane modification for defect passivation and stability enhancement of high-efficiency perovskite solar cells, J. Phys. Chem. C 124 (2020) 22903–22913, https://doi.org/10.1021/acs.jpcc.0c05649.